The Plant Cell, 2026, 38, 1–21
https://doi.org/10.1093/plcell/koag120
Published: 21 April 2026
Research article

A four-dimensional spatial transcriptome atlas of barley caryopsis development and germination

Marta Peirats-Llobet [1,2], Zorana Staka [1,3], Xiujuan Yang [4], Yanqiao Zhu[1,3], Cunman He [1,3], Bhavna Hurgobin [2,5], Felipe Ayora [6,7], Maria Sofia L. Yangzon [6,7], Monika W. Murcha [8], Valencia Marisa [8], Ghazanfar Abbas Khan [9], Runxuan Zhang [10], Iain Milne [10], Huixia Shou [1,3], Matthew R. Tucker [4], Mathew G. Lewsey [2,5,11]*, and James Whelan [1,3]*

[1]State Key Laboratory of Plant Environmental Resilience, College of Life Science, Zhejiang University, Hangzhou, Zhejiang 310058, P.R. China

[2]Department of Ecological, Plant and Animal Sciences, La Trobe Institute for Sustainable Agriculture and Food, School of Agriculture, Biomedical and Environmental Sciences, La Trobe University, Bundoora, Victoria 3086, Australia

[3]The Provincial International Science and Technology Cooperation Base on Engineering Biology, International Campus of Zhejiang University, Haining, Zhejiang 314400, China

[4]Waite Research Institute, School of Agriculture, Food and Wine, The University of Adelaide, Waite campus, Adelaide, South Australia 5064, Australia

[5]Australian Research Council Research Hub for Protected Cropping, AgriBio, La Trobe University, Melbourne, Victoria, Australia

[6]BizData, Melbourne, VIC 3000, Australia

[7]Research and Advanced Computing, BizData, Wellington 6011, New Zealand

[8]School of Molecular Sciences, The University of Western Australia, Crawley, Western Australia 6009, Australia

[9]School of Life and Environmental Sciences & Centre for Sustainable Bioproducts, Deakin University, Waurn Ponds, VIC, Australia

[10]Department of Information and Computational Sciences, The James Hutton Institute, Invergowrie, Dundee, Scotland

[11]Australian Research Council Centre of Excellence in Plants for Space, AgriBio, La Trobe University, Melbourne, Victoria, Australia

*Corresponding authors: James Whelan, State Key Laboratory of Plant Environmental Resilience, College of Life Science, Zhejiang University, Hangzhou, Zhejiang 310058, P.R. China; The Provincial International Science and Technology Cooperation Base on Engineering Biology, International Campus of Zhejiang University, Haining, Zhejiang 314400, China. Email: jimwhelan@zju.edu.cn; Mathew G. Lewsey, Department of Ecological, Plant and Animal Sciences, La Trobe Institute for Sustainable Agriculture and Food, School of Agriculture, Biomedical and Environmental Sciences, La Trobe University, Bundoora, Victoria 3086, Australia; Australian Research Council Research Hub for Protected Cropping, AgriBio, La Trobe University, Melbourne, Victoria, Australia; Australian Research Council Centre of Excellence in Plants for Space, AgriBio, La Trobe University, Melbourne, Victoria, Australia. Email: m.lewsey@latrobe.edu.au.
The authors responsible for distribution of materials integral to the findings presented in this article in accordance with the policy described in the Instructions for Authors (https://academic.oup.com/plcell/pages/General-Instructions) are Jim Whelan, jimwhelan@zju.edu.cn, and Mathew G. Lewsey, m.lewsey@latrobe.edu.au.

Abstract

A 4-dimensional spatial gene expression atlas of *Hordeum vulgare* (barley) grain development and germination was generated using spatial transcriptomic analysis of serial sections to reconstruct transcript abundance in 3 physical dimensions and with temporal kinetics. We investigated the subtissue localizations of specific biological activities, using energy biology as an example, including genes encoding proteins involved in starch synthesis and degradation, sugar transport, and mitochondrial and chloroplast activity. This atlas revealed different patterns in gene expression across tissues and developmental stages. Heterogeneity in gene expression was observed between clusters, within domains of the individual clusters, across 2-dimensional (xy, 55-μm resolution) and 3-dimensional (xyz, 8-μm resolution in z-plane) axes. Yet, other genes, including typical housekeeping genes such as *Actin*, *Tubulin*, and others, display homogeneous expression patterns. Expression of several genes matched previous gene-specific studies in different barley varieties verifying the robustness of the approach and indicating that patterns of gene expression are conserved at least for some categories of genes between varieties. Trajectory analysis of aleurone tissue spanning from early development to the completion of germination, provided a comprehensive roadmap of tissue development in terms of processes and identified transcription factors with spatial specificity that play roles in seed development and germination. A public visualization browser is available to view 2- and 3-dimensional transcription abundance profiles at https://barley-4d.latrobe.edu.au/or https://barley-4d-gene-atlas.hutton.ac.uk/.

Received: August 12, 2025. **Accepted:** March 7, 2026

Introduction

Seed development and germination are fundamental biological processes that shape the productivity of agricultural systems and the resilience of natural ecosystems. Seeds provide a reservoir for continuous cultivation, securing the global food supply, while seed dormancy underpins ecological stability by allowing plants to withstand adverse conditions (Basto et al. 2015; Eskelinen et al. 2021). Seeds from cereals and legumes together contribute approximately 70% of the global caloric intake, with cereals contributing approximately 45% of calories (Poutanen et al. 2022; Bellamy et al. 2024). Among these, barley (*Hordeum vulgare*) stands as the fourth most cultivated cereal, playing a pivotal role in human and livestock nutrition and serving as a key resource for the food and beverage industries.

Barley grain formation occurs across a window of approximately 40 d post-anthesis. The architecture comprises the diploid embryo, formed from fusion of an egg and sperm nucleus, with a body plan including the coleoptile, plumule, shoot apical meristem, radicle, coleorhiza, and scutellum; the triploid endosperm, originating from the fusion of the diploid central cell nucleus and a second sperm nucleus, which differentiates into structurally and functionally distinct domains such as the central starchy endosperm, aleurone layer, embryo-surrounding region, and endosperm transfer cells; and the surrounding maternal tissues, the pericarp and seed coat layers, that regulate nutrient transfer, protect the embryo, and contribute to early starch reserves (Olsen 2001). Barley seed development progresses through pre-storage, storage, and desiccation phases, each marked by specific morphological changes, shifts in metabolite accumulation, and transcriptional reprogramming, ultimately equipping the seed for successful germination (Kovacik et al. 2024). However, the detailed molecular mechanisms governing these transitions, particularly at spatial and temporal resolution, remain poorly understood.

Traditional whole-grain transcriptome profiling, initially employing microarrays and subsequently RNA sequencing (RNA-seq), has helped elucidate key metabolic and regulatory processes, including carbohydrate metabolism, hormonal signaling, and organelle development (Sreenivasulu et al. 2008; Betts et al. 2020; Auroux et al. 2025). However, such bulk approaches lack the spatial and quantitative resolution inherent within individual cell types and tissues. Emerging single-cell and single-nuclei RNA-seq technologies have addressed many of these limitations, enabling the characterization of cell type–specific transcriptional profiles across various plant species and tissues (Minow et al. 2023; Oliva and Lister 2023; Nobori 2025). Furthermore, single cell multi-omic approaches are now emerging combining analysis of transcriptomes with regulatory elements to give greater insight on cell-specific *cis* regulation and the evolution of regulatory processes (Li and Schmitz 2025; Marand et al. 2025; Yan et al. 2025). While these approaches have made step-change advances in our understanding of development, they lose the native spatial organization of gene expression critical to understanding development, metabolism, and stress responses.

Spatial transcriptomics now offers a transformative means to capture gene expression within intact tissue sections. Initially applied in model species like *Arabidopsis thaliana* (Giacomello et al. 2017; Moreno-Villena et al. 2022; Liu et al. 2022a; Xia et al. 2022), spatially resolved approaches are increasingly deployed in cereals. Recent studies have leveraged these methods to investigate barley grain germination (Peirats-Llobet et al. 2023), rice germination (Yao et al. 2024), and maize kernel development (Fu et al. 2023). Spatial transcriptomics combined with single-cell/nuclei RNA-seq have been used to define and verify cell markers in Arabidopsis and soybean (Guo et al. 2025b; Lee et al. 2025; Zhang et al. 2025), and the spatial responses to biotic challenges (Nobori et al. 2025; Wang et al. 2025), illustrating the need for multiple approaches in single cell transcriptome approaches.

Here, we apply spatial RNA-seq to generate a high-resolution, temporally resolved transcriptomic atlas of barley grain development and germination. We sequentially sectioned barley seeds at various developmental and germination stages, allowing transcript abundance to be mapped in 2-dimensional (2-D) tissue sections and reconstructed into a comprehensive 3-dimensional (3-D) model. Integrating these data across developmental time points enabled us to generate a detailed 4-dimensional (4-D) view of transcriptomic dynamics.

Glossary

Spatial cluster is a group of spots with similar expression profiles, identified through unsupervised clustering methods.

Organ describes a complex structure composed of multiple types of tissues working together to perform one or more functions. Examples are embryo, endosperm, aleurone layer, plumule, roots, seed coat, and pericarp.

Tissue describes a group of cells with similar structures and functions that work together to perform a specific role in the plant. Tissues are categorized into meristematic and permanent according to their differentiation rate, actively differentiating in the case of meristematic tissues and fully differentiated for permanent tissues. Permanent tissues can be further classified as simple (containing only 1 cell type) or complex (containing multiple cell types). Examples are scutellum, coleoptile, coleorhiza, starchy endosperm, aleurone cells, nucellar projection, vascular bundle, pigment strand, and husk.

Cell types are groups of specialized cells that share similar structural and functional characteristics. Plant cell types are differentiated to perform specific roles within a plant tissue. Examples include phloem cells, vasculature cells, and chlorenchyma cells.

Domains describe (in this paper) groups of spots within a tissue that have a specific gene expression pattern, but which do not include all the spots within a cluster/organ/tissue.

Results

Establishing a 4-D spatial transcriptomic atlas of barley grain from development to germination

To construct a high-resolution spatial transcriptomic atlas of barley (*Hordeum vulgare* cv La Trobe) grain development and germination, we generated 2 complementary datasets (Fig. 1) in addition to our previously generated longitudinal germination dataset (Peirats-Llobet et al. 2023). The developmental dataset comprised 4 longitudinal serial sections per time point (8 μm thick, named A, B, C, and D as per the Visium captured areas) sampled at 3, 6, 12, and 20 d after pollination, covering syncytial, cellularization, early and late storage phases, respectively (Fig. 1a and b). The germination transverse dataset consisted of 8 transverse serial sections per time point (8 μm thick, named A, B, C, and D as per the Visium captured areas) collected at 0 (dry grain), 1, 3, 6, and 24 h after imbibition, encompassing

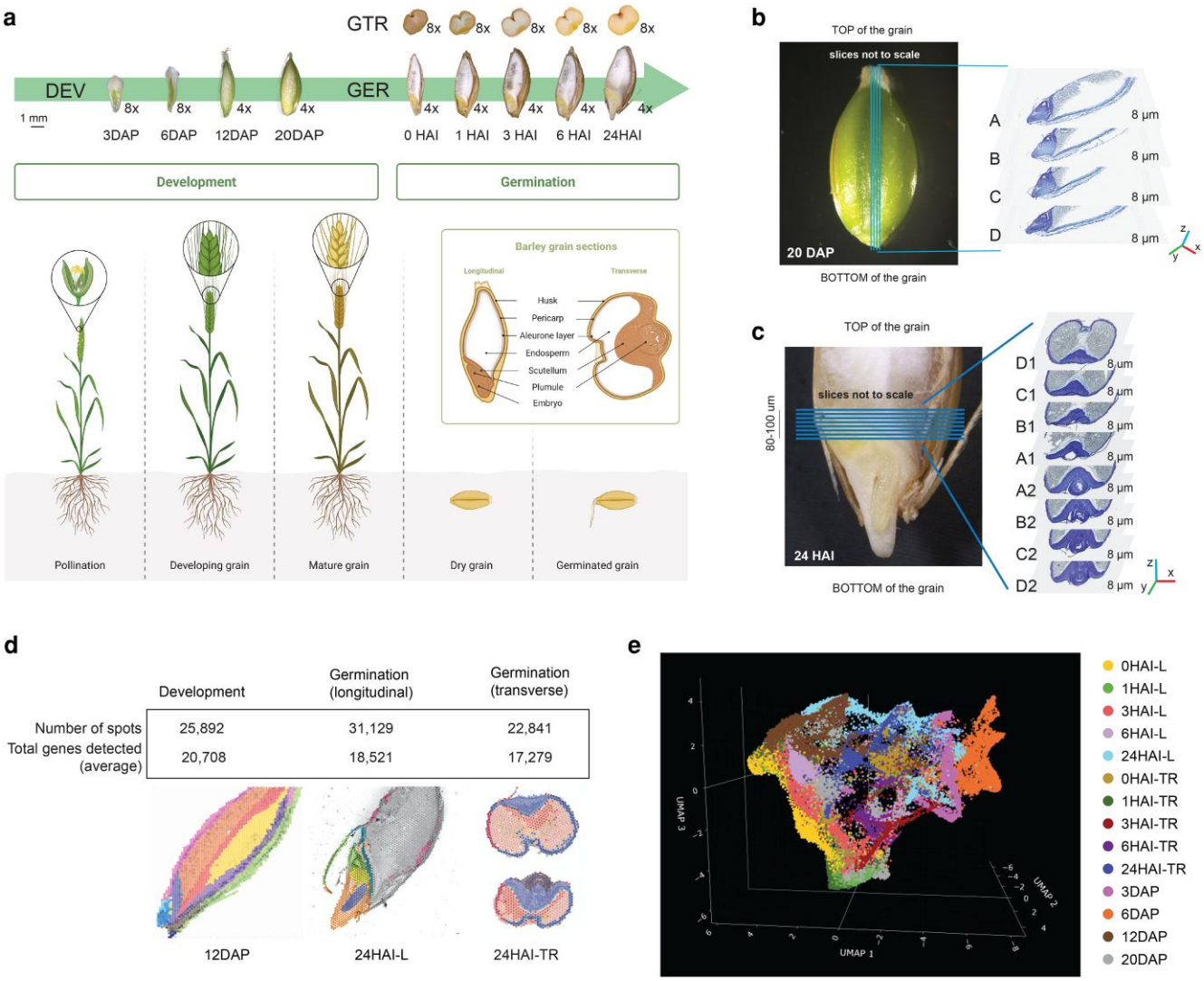

Figure 1 Generating a 4-D spatial transcriptome barley grain atlas. a) Overview of the sampling numbers and times in grain development and germination to generate the 4-D spatial barley grain atlas. b) Representation of our experimental design for the development samples showing 4 sections (named from A to D as per their position on the Visium slide), to facilitate 3-D reconstruction of the pattern of gene expression. Slices not to scale. c) Representation of our experimental design for the germination transverse samples, with 8 serial sections (named from A to D as per their position on the Visium slide), to facilitate 3-D reconstruction of the pattern of gene expression. Slices not to scale. d) Spatial transcriptomics metrics across our experimental datasets. The longitudinal germination dataset is from Peirats-Llobet et al. 2023. e) 3-D UMAP graph colored by time point—see HTML file S1 for interactive graph. Abbreviations: DAP, days after pollination; HAI, hours after imbibition; L, longitudinal; TR, transverse.

imbibition and stationary phases (Fig. 1a and c). In total, this study consisted of 84 sections: 24 from the developmental series, 40 from germination transverse series, and 20 from the previously published germination dataset (Peirats-Llobet et al. 2023). Serial sectioning provided "replicates" for each time point and allowed us to reconstruct a third dimension (*z*-axis) in our analysis (Fig. 1b and c) and, when combined with the temporal axis, enabled the construction of a barley 4-D grain atlas.

The development dataset yielded 25,892 spots located under tissue, encompassing 20,708 expressed genes, with an average of 1,463 genes per spot. The germination transverse dataset contained 22,841 spots under tissue, covering 17,279 expressed genes, with an average of 558 genes per spot (Fig. 1d, Table S1). For quality control, per-spot metrics such as transcript and gene density distributions, were plotted for both datasets (Figs. S1 and S2). A higher number of unique molecular identifiers (UMIs) and genes were detected in the embryonic regions of both datasets, consistent with their known complexity (Figs. S1 and S2). Low number of UMIs and genes were detected for 0 h after imbibition in germination transverse dataset, possibly due to the dry nature of the samples (Fig. S2). As a second quality control step for the number of UMIs and genes in our samples, we plotted 6 genes for each group of datasets, development (Fig. S3) and germination (Fig. S4) that illustrated the diversity in gene expression patterns. The patterns diverged from uniform, in the case of non-specific lipid transfer protein 3 (*nsLTP3—HORVU2Hr1G107480*) and seed storage 2S protein (*HORVU5Hr1G046550*), to mottled expressions, such as the *SWEET4* (*HORVU6Hr1G055960*), *HvSWEET15a* (*HORVU7Hr1G030160*), and granule bound synthase (*GBSS1b—HORVU2Hr1G090980*) genes. To further assess the quality of the datasets, we generated scatter plots for each section, to visualize the

relationship between the number of UMIs/library size (nCounts) and number of genes per spot (nFeatures) (Figs. S5–S13). The plots showed upwards curves indicating a saturation pattern commonly found in biological samples. We also plotted the library sizes across the spots per section which fit the expected size distribution for spatial data (Figs. S5–S13) (https://satijalab.org/seurat/articles/pbmc3k_tutorial#standard-pre-processing-workflow and https://bookdown.org/sjcockell/ismb-tutorial-2023/practical-session-2.html#spot-level-quality-control).

To evaluate dataset reproducibility, we performed correlation analyses on replicate sections from each time point (Figs. S14 and S15). Correlation coefficients ranged from 0.997 to 0.943 in development and 0.997 to 0.970 in germination transverse datasets. These correlations are very similar to results obtained for spatial transcriptome data generated using a different platform (Yao et al. 2024). They may appear high relative to correlations obtained in tissue-specific studies using bulk RNA sequencing methods, but this reflects the fact that sections in our study are from a single developing or germinating seed compared with tens of seeds that are used in bulk RNA sequencing of dissected tissues. The relatively high correlations may also be due to the very precise tissue sampling (tens of microns of tissue) as opposed to the bulk studies (Fig. 1b and c).

Next, we compared our spatial transcriptomic data with previously published bulk transcriptomic analyses of barley grain development and germination. Manual dissections of embryo, starchy endosperm, and seed maternal tissues in prior work (Kovacik et al. 2024) detected just over 21,000 expressed genes with a cut-off of >10 TPM (Kovacik et al. 2024). Our development dataset identified over 20,000 genes after removing spots with <200 UMI counts and <150 genes per spot, which represents only a few cells (Fig. 1d, Fig. S16A). Our detection of expressed genes is comparable to the previous study, particularly considering that we sampled only 32 μm of tissue (four sections) at each time point, in contrast to whole tissues from several grains used for bulk sequencing. Thus, all the tissues in the grain were not sampled in our study (Fig. 1b and c). We also verified whether we could detect genes that fell below the 10 TPM threshold in the previous study, and we found we could detect genes with expression as low as 0.1 TPM (Fig. S17, Table S2). For example, *β-glucosidase 29* gene was expressed at a very low level (mean TPM of 0.2 to 0.8 in some tissues and time points) was detected in our study, even in tissues where it was not detected in the previous study (Kovacik et al. 2024). For germination, manual dissections identified over 30,000 genes (Betts et al. 2020), while our combined spatial germination datasets (longitudinal and transverse) detected ~28,000 genes (Fig. S16A).

A global comparison of the datasets revealed approximately 80% gene overlapping of expressed genes between the newly generated germination transverse data and our previous germination dataset (Peirats-Llobet et al. 2023), and around 85% overlap between the combined germination datasets and the development dataset (Fig. S16A). A 3-D UMAP representation of samples showed a continuum of clusters as might be expected from the high overlap in gene expression observed (Fig. 1e; HTML file S1, https://barley-4d.latrobe.edu.au/ or https://barley-4d-gene-atlas.hutton.ac.uk/). Intersection analyses indicated that individual development datasets shared most of their expressed genes, with a small fraction being unique. The germination transverse datasets also shared most genes; however, ~2,000 genes were uniquely expressed in imbibed samples and absent in the dry seed (0 h after imbibition) (Fig. S16B). This may be due to the low number of genes detected at 0 h after imbibition. We detected the fewest genes (~10,000) at 0 h after imbibition, likely due to the anhydrous state of the tissue and high starch content impacting oligonucleotide binding efficiency. However, we highlight that transcription is rapidly initiated upon imbibition and results in upregulation of many thousands of genes (Narsai et al. 2017; Tremblay et al. 2024). Nevertheless, the 0 h after imbibition dataset was retained as it still provided valuable information on the quiescent state of the seed.

Overall, our spatial transcriptomic approach yielded a level of gene detection broadly comparable to that of bulk tissue transcriptomes, while providing insights into the spatial and temporal dynamics of gene expression.

Spatial transcriptomics unveil gene expression heterogeneity between and within clusters, organs, tissues, and domains during barley seed development and germination

As spatial transcriptomic data includes coordinates for gene expression, unsupervised clusters could be directly overlaid onto brightfield images to define organs, tissues and domains (view glossary). This identified 41 clusters across grain development (Fig. 2a and b). The early time points of development, the pre-storage phase (3 and 6 d after pollination) were defined by relatively simple caryopsis structures (i.e. a thick pericarp surrounding the embryo sac), and shared pericarp clusters 31 and 7 (Fig. 2a), pointing to shared transcriptional states in early grain development. Interestingly, this design and resolution allowed us to define the epidermis at 6 d after pollination by 2 clusters, top and bottom epidermal layers (cluster 38 and 10, respectively). Later developmental stages (12 and 20 d after pollination) were subdivided into intermediate (12 d after pollination) and late storage phases (20 d after pollination), where the seed had enlarged, the pericarp had undergone programmed cell death and distinct embryo structures were identified (Fig. S18). The starchy endosperm resolved into different clusters at 12 and 20 d after pollination. Clusters 12 and 15 were defined as starchy endosperm at 12 d after pollination and clusters 8 and 9 at 20 d after pollination. These clusters identified different domains of gene expression within the same tissue but also indicated that gene expression within the starchy endosperm changed from 12 to 20 d after pollination. Moreover, the power of spatial transcriptomics identified cell types as individual clusters—for example, vascular bundle in cluster 34 and chlorenchyma in clusters 36 and 33, and organs such as coleorhiza in cluster 27 and scutellum in cluster 28. The serial sections and clusters for each time point are shown in Figures S18 and S19.

A combination of histological images, literature-based marker genes, and in silico-identified markers (Fig. S20) were used to annotate clusters. The analysis of 12 d after pollination was chosen as an example of the annotation (Fig. 2b and c). For each cluster, in silico marker genes were identified and their transcriptional abundances are displayed at the bottom of the figure (Fig. 2c). Transcriptional abundances of some marker genes were quite distinct, displaying homogeneous expression within the clusters as in the case of endosperm adjacent to scutellum (EAS)—*Serine carboxypeptidase 2*, and endosperm transfer cells (ETC)—*Autophagy-related protein 4*, while others displayed some variation over the cluster, in the embryo—*Delta 1-pyrroline-5-carboxylate synthetase* and starchy endosperm—*Thiamine thiazole synthase 2*, which were higher in some regions of the cluster (Fig. 2c).

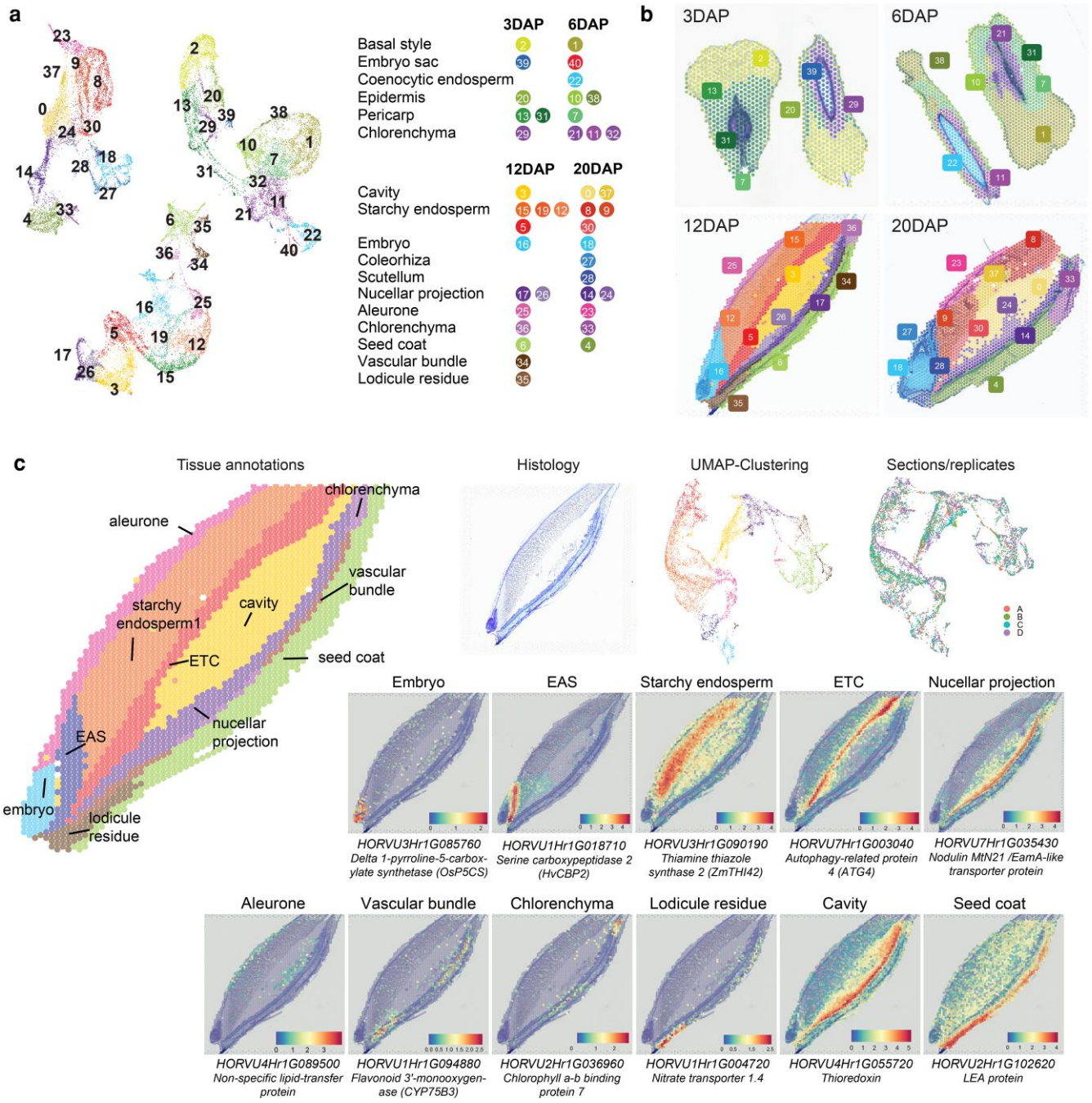

Figure 2 Time course analysis for barley grain development. a) Dimensionality reduction and clustering graph of the combined development datasets colored by cluster with tissue annotations. b) Bright field images overlapped with spatial spots. c) Overview of tissue annotations over spatial spots, toluidine blue stained brightfield imagen (see Fig. S18), UMAP clustering, sections/replicates and marker genes with IDs for barley grain development at 12 d after pollination (section A). See Figure S20 for 3, 6, and 20 d after pollination. Abbreviations: DAP, days after pollination; EAS, embryo adjacent to scutellum; ETC, endosperm transfer cells.

A similar clustering strategy was applied to the germination transverse dataset. The combined analysis and clustering of all the germination transverse timepoints identified 27 clusters (Fig. 3a, Fig. S21 all sections) and their corresponding location on the brightfield images (Fig. 3b). Unsupervised clustering identified most tissues as belonging to the same clusters in the 2 sections in the germination transverse dataset. The UMAP by time suggested that the transcriptomes were similar across time points, as would be expected given the narrow temporal intervals when compared with the grain development data (hours rather than days) (Fig. 3c). Clustering without the 0 h after imbibition produced 29 clusters with a UMAP displaying a similar pattern, verifying that the relatively low detection of transcripts at this timepoint was not notably affecting analyses of later timepoints (Fig. S22). For the downstream analysis, we retained the 0 h after imbibition timepoint because transcript abundances were visualized on the sections as *Z*-scores of counts per spot. Individual

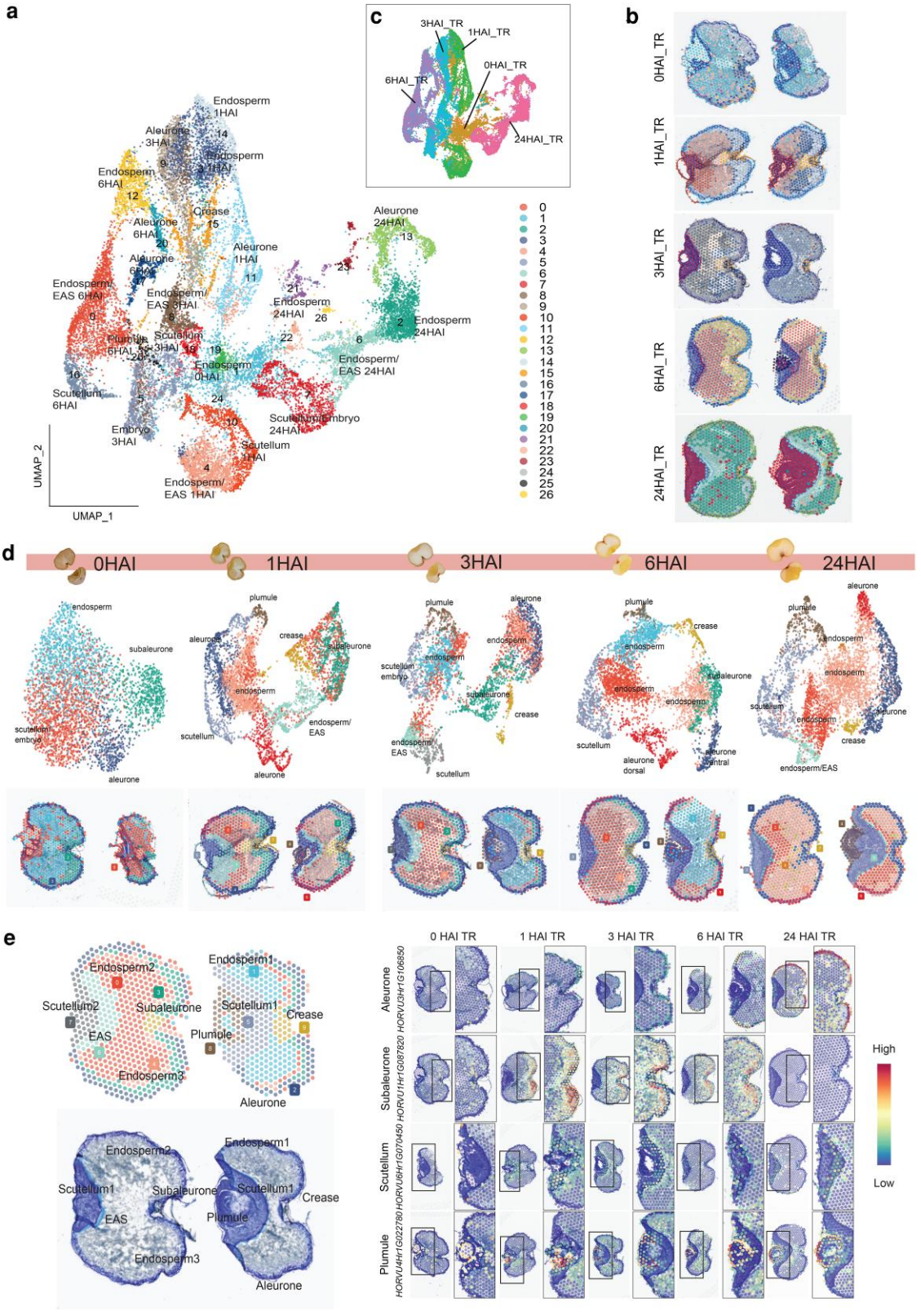

Figure 3 Time course analysis for barley grain germination (transverse). a) Dimensionality reduction and clustering (UMAP) graphs of the combined germination transverse datasets colored by cluster with tissue annotations. b) Brightfield images overlapped with spatial spots clustered and annotated at all time points. c) UMAP colored by time point. d) Dimensionality reduction plots (top) and spatial images overlapped with clusters (bottom) for each time point analyzed individually. e) Marker genes for barley grain germination. Representative spatial image (top left) and brightfield image of the same time point (bottom left) with labeled and annotated clusters. Spatial gene expression of 4 representative marker genes (right). See Figure S11 for marker gene bubble plots of 0, 1, 3, 6, and 24 h after imbibition. Abbreviations: HAI, hours after imbibition; TR, transverse.

datasets corresponding to the different time points were used for the tissue annotation (Fig. 3d) and marker gene analysis (Fig. S23). Time point-specific marker gene identification revealed that certain genes remained robust tissue-specific markers across time (Fig. 3e). For example, aleurone marker, *HORVU3Hr1G106850*, could be detected in a few of the spots in the cluster as early as 0 h after imbibition and the expression increasing all the way to 24 h after imbibition. Subaleurone marker, *β-hordothionin* (*HORVU1Hr1G087820*), transcript abundance was mainly detected in the intermediate time points (1, 3, and 6 h after imbibition) with gradients of expression across the spots in the cluster. The scutellum marker, putative nitrate transporter (*HORVU6Hr1G070450*), and plumule marker, *HORVU4Hr1G022780*, on the other hand, despite showing a continuous expression across the time course, had a heterogeneous pattern where not all the spots in the cluster displayed the same level of expression. These observations contrast with the developmental datasets, where overlapping gene expression during tissue formation and differentiation was not encountered. This stability in germination markers again reflect the narrower temporal intervals and the fact that cell identities are already established early in development (Armenta-Medina et al. 2021).

Transcript abundance of starch metabolism genes in barley grain reveals a heterogeneous mosaic pattern during development and germination

Starch is the primary component of cereal grains, and its metabolism during development and germination has been extensively investigated (Radchuk et al. 2009; Huang et al. 2021; Liu et al. 2022b) for its significance in malting and brewing (Bewley et al. 2013; Rani and Bhardwaj 2021). Therefore, we explored this intensively studied pathway to investigate if spatial transcriptomics could give insights or avenues of investigation that are currently unknown. We generated a bubble plot that provided a general overview of starch metabolism and showed that both starch synthesis and degradation genes were expressed from the earliest stages of grain development (Fig. S24). Some genes are highly expressed (e.g. *α-glucosidase 1*, *AGL1*, *HORVU7Hr1G106540*) early in development in the pericarp at 3 and 6 d after pollination, which has not been previously detected, with lower expression levels during storage phases and later during germination. Still at 24 h after imbibition, *AGL1* is highly expressed again in aleurone and scutellum (Figs. S25–S27). Also, *AMY1_1a*, *HORVU6Hr1G078330*, in a specific area of the ETC at 12 d after pollination and again in very specific area in the EAS at 24 h after imbibition (Figs. S28–S30). *AMY1_1a* expression is often detected in a limited number of spots (subset of cells), indicating heterogeneous expression patterns consistent with the expression patterns detected in the overall analysis of transcript abundance of starch genes (Fig. S24). This quantitative detection of starch metabolic genes at early developmental stages 3 and 6 d after pollination, with specific spatiotemporal patterns, reveals previous unknown complexity and dynamic regulation underlying starch metabolism at a cellular scale.

To gain further understanding of the spatial pattern of gene expression, we focused on 2 granule-bound starch synthase genes (*GBSS1a* and *GBSS1b*), which are crucial for amylose chain elongation (Fig. 4a). During development, *GBSS1b* is abundant in maternal tissues (pericarp) at 3 and 6 d after pollination, whereas *GBSS1a* is expressed at low but detectable levels. At 12 and 20 d after pollination, *GBSS1a* becomes highly expressed in the starchy endosperm, while *GBSS1b* predominates in the embryo. During germination, *GBSS1a* is strongly detected in the subaleurone at 1, 3, and 6 h after imbibition and to a lesser extent in the starchy endosperm and crease (Fig. 4a and b, HTML File S2). In contrast, *GBSS1b* appears most strongly in the plumule and to a lesser extent in the scutellum and embryo adjacent scutellum (EAS) region at 1 h after imbibition, before declining to undetectable levels by 24 h after imbibition (Fig. 4a and c, HTML File S3). To easily visualize these expression patterns, we utilized the 2-D spatial images and the serial sectioning design (Fig. 1b and c) and reconstructed a z-stack (3-D) using 4 or 8 serial sections per time point in development and germination transverse, respectively. During development, *GBSS1a* at 3 d after pollination appears in small foci at the proximal end of the style (black arrows, Fig. 4b, HTML File S4). At 6 d after pollination, similar foci are present in the coenocytic endosperm (black arrows, Fig. 4b, HTML File S4). By 12 d after pollination, *GBSS1a* is distributed throughout the starchy endosperm, while at 20 d after pollination it is abundant in clusters associated with the endosperm (Fig. 4b). For *GBSS1b* at 3 d after pollination, a front view shows expression surrounding the embryo sac, with higher intensity in the top sections, while a side view places this expression in the pistil epidermis and chlorenchyma (Fig. 4c, HTML File S5A). At 6 d after pollination, its expression forms distinct foci in the pericarp, and by 12 d after pollination it localizes to the embryo (black arrows), diminishing further by 20 d after pollination (HTML File S5B–D). During germination, *GBSS1a* at 1 h after imbibition, showed high expression levels largely confined to the subaleurone (Fig. 4b, HTML File S2A, B). This pattern persists at 3 and 6 h after imbibition, with slightly higher expression in the upper sections, and by 24 h after imbibition only isolated hotspots remain (HTML File S2C–E). For *GBSS1b*, expression is even more focal. At 1 h after imbibition, it is detected in the plumule and scutellum, particularly in the lower 4 sections (Fig. 4c, HTML File S3A). By 3 h after imbibition, plumule expression persists and spreads to the starchy endosperm in discrete foci (HTML File S3B). Expression declines at 6 and 24 h after imbibition, leaving only a few distinct foci (HTML File S3C, D). These results suggested that *GBSS1* genes show compartmentalized expression in time and space (maternal vs filial).

Given that starch metabolism is intensively studied in cereal grains, we examined whether the literature on starch synthesis and degradation aligns with the spatiotemporal patterns we detected, acknowledging that different varieties, environmental conditions and techniques used may result in some variation. The α-amylase activity in developing barley caryopsis was predominantly located in the pericarp, and starch granule degradation strongly coincided with amylase activity. The β-amylase enzyme activity could be detected in the barley endosperm at later developmental stages (Radchuk et al. 2009 and references therein). This general pattern is consistent with the spatiotemporal patterns detected in this study.

To analyze this spatial variation of the expression patterns further, we reconstructed 3-D transcript abundance for 2 other starch-related genes during germination and performed a section analysis. *β-amylase 1* (*BAM1*), critical for starch breakdown, illustrates that transcript abundance can differ substantially between distal and proximal sections relative to the embryo, creating a heterogeneous 3-D expression pattern (Fig. 4d, HTML File S6). Similar patterns emerge for starch binding enzyme1 (*SBE1*). *SBE1*, which promotes maltose-oligosaccharide extension (Cuesta-Seijo et al. 2017), shows subaleurone tissue enrichment with distinct top-to-bottom section differences (Fig. 4e, HTML File S7).

We examined additional genes, including but not limited to, typical housekeeping genes such as actin and tubulin to gain a wider view of

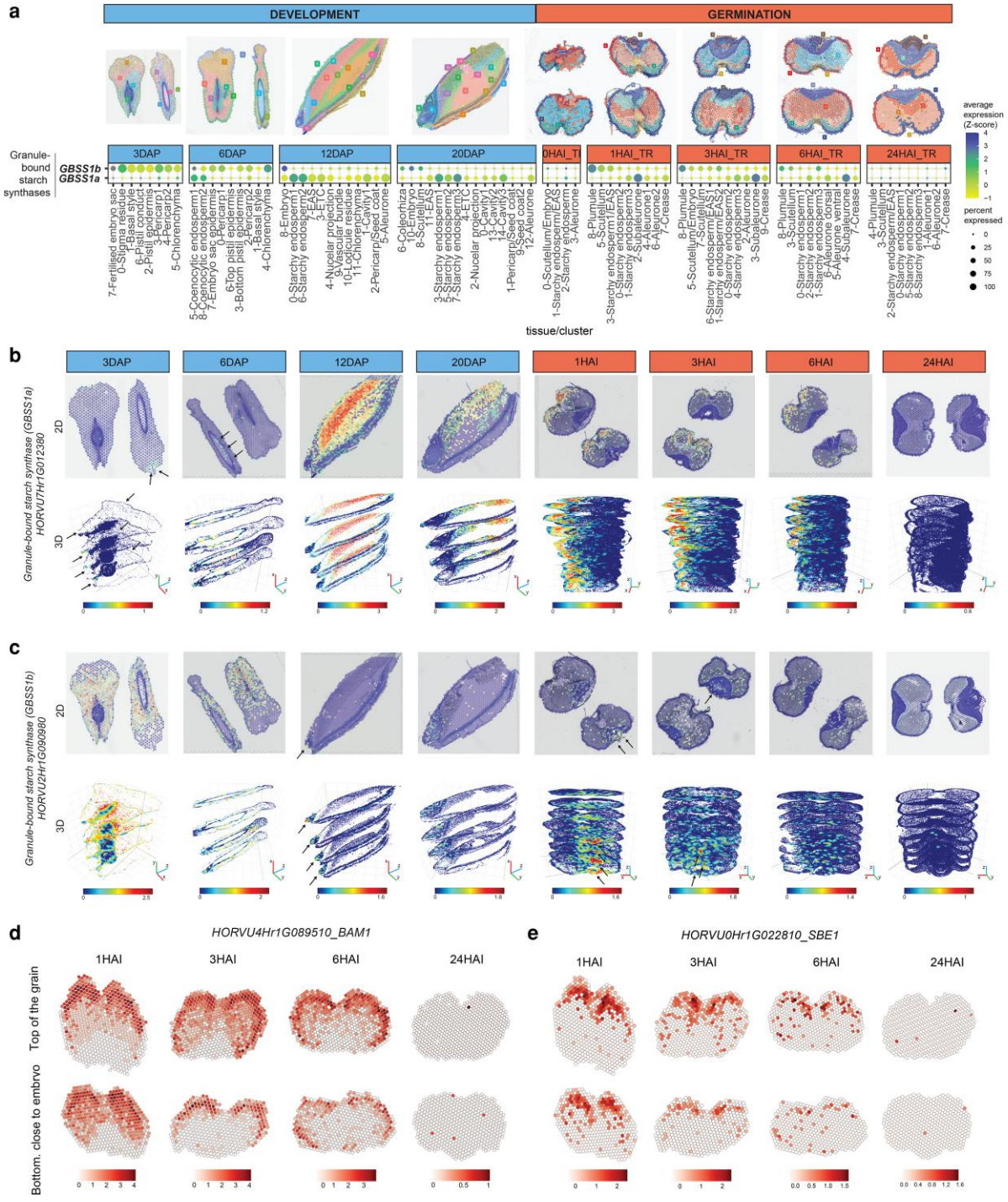

Figure 4 A spatial view of starch metabolism across development and germination. a) The top panel represents the cluster analysis at each time point as defined in Figures 2 and 3 for grain development and germination respectively. The lower panel is a bubble plot representation of transcript abundance of starch metabolic genes, encoding granule-bound starch synthases 1 a and b, across the development and germination transverse datasets. Color scale corresponds to the average gene expression across the spots per cluster and the circle size indicates the percentage of spots expressing a gene within the cluster. b, c) Spatial gene expression in 2-D (top) and 3-D reconstructions (bottom) of *GBSS1a* (b) and *GBSS1b* (c) transcriptome abundances. Black arrows indicate the location of transcripts. d) Transcript abundance of *BAM1* expression of the top and bottom sections of the z-stack at the different time points (left panels) and 3-dimension reconstruction of *BAM1*, with the 8 sections from the 3 h after imbibition time point showing heterogeneous expression in the z-stack. (See HTML file S6 for reconstructions at all germination time points or visualize in the database by inputting the gene ID at https://barley-4d.latrobe.edu.au/ or https://barley-4d-gene-atlas.hutton.ac.uk/. e) Transcript abundance of *SBE1* expression of the top and bottom sections of the z-stack at the different time points (left panels) and 3-D reconstruction of *SBE1*, with the 8 sections from the 3 h after imbibition time point show heterogeneous expression in the z-stack. (See HTML file S7 for 3-D reconstructions at all germination time points or visualize in the database by inputting the gene ID at https://barley-4d.latrobe.edu.au/ or https://barley-4d-gene-atlas.hutton.ac.uk/. Abbreviations: DAP, days after pollination; HAI, hours after imbibition; ETC, endosperm transfer cells; EAS, embryo adjacent to scutellum; GBSS, Granule-bound starch synthase.

expression patterns (Fig. 5). For development, we show the 3-D pattern of expression of genes encoding *Actin* and *Tubulin* isoforms. While there are tissue or subtissue differences in gene expression levels, expression is largely consistent along the *Z*-axis (Fig. 5a). Similarly, for germination, a consistent pattern is observed in 3-D for genes encoding *Metallothionin*, a *Late Embryogenesis Abundant protein* (*LEA*) and *a Non-specific Lipid transfer protein* (*nsLTP*). The gene encoding a metallothionin isoform is widely expressed, especially in the aleurone, scutellum, and endosperm, and shows consistent expression within tissues in both 2-D and 3-D. The gene encoding a *LEA* protein peak in expression at 1 h after imbibition and, although somewhat variable in the 2-D, remains relatively consistent in the *Z*-axis. The gene encoding the *nsLTP* is more restricted to the plumule but displays homogeneous expression in both 2-D and 3-D (Fig. 5b).

SWEET genes display distinct 2-D and 3-D transcript abundance patterns

Next, we examined members of the SWEET gene family that are essential for sugar transport during barley grain development and germination. *OsSWEET11* and *OsSWEET15* affect grain filling in rice (Kong et al. 2022). In barley, *HvSWEET1a* and *HvSWEET4* are highly expressed in the aleurone layer and scutellum during germination (Yue et al. 2023). Our analysis of *HvSWEET4* (*HORVU6Hr1G055960*) showed expression during development, in the pistil at 6 d after pollination, chlorenchyma, ETC, and aleurone at 12 d after pollination and in the seed coat/integuments at 20 d after pollination (Fig. 6a visualized in 3-D during development, 2-D in Fig. S31, HTML File S8). During germination expression was observed in the aleurone layer and scutellum at all post-imbibition time points (Fig. 6a visualized in 3-D during germination, 2-D in Figs. S31–S33, HTML File S8). Although some variation was noted along the *z*-axis, particularly with 1 aleurone lobe displaying higher expression in the upper sections, its overall distribution was homogeneous within single sections and across sections compared with starch-related genes. *HvSWEET11b*, which transports sugar and cytokinin, influences grain size, sink strength, and endosperm endopolyploidy, as well as starch and protein content (Radchuk et al. 2023), exhibited spatially and temporally restricted expression patterns. Its expression pattern was consistent and tissue specific (notably in the nucellar projection at 12 and 20 d after pollination) (Fig. 6b, HTML File S9) and aligned with previous RT-qPCR and in situ hybridization studies (Radchuk et al. 2023). *HvSWEET15a* was found to be expressed in embryonic tissues throughout development (Fig. 6c development) and at different levels in aleurone and starchy endosperm during germination (Fig. 6c germination, HTML File S10).

The examples of *HvSWEET4, 11b*, and *15a* demonstrate that the spatial patterns we observed are consistent with previous independent studies, providing external validation of the patterns determined in this study. Additionally, while some variation was evident, the expression patterns were more consistent between sections for these genes compared with those associated with starch metabolism.

Differential, dynamic, and domain expression of transcripts encoding energy organelle proteins during barley grain development and germination

Macromolecular carbohydrate metabolism of starch synthesis is underpinned by mitochondrial and plastid (chloroplast) functions during development and germination with the importance of oxygen and ATP having been previously documented for starch accumulation during grain development in barley (Rolletschek et al. 2004; Bewley et al. 2013). Mitochondrial biogenesis during germination has also been extensively studied at both a transcriptome and protein level, together with activity measurements from whole embryos in maize, rice, barley, and Arabidopsis (Logan et al. 2001; An and Lin 2011; Law et al. 2012; Paszkiewicz et al. 2017; Zhu et al. 2020; Collins et al. 2021; Kovacik et al. 2024).

During development, high transcript abundance for mitochondrial biogenesis and activity was evident from 3 d after pollination (pre-storage) through 12 d after pollination (intermediate phase), followed by a marked decline by 20 d after pollination (late storage phase) (Fig. S34, Table S3). Although transcripts for these functions were often abundant across a range of clusters, they appeared only in subsets of cells (spots), especially at 20 d after pollination. Notably, embryo, and to a lesser extent coleorhiza, scutellum, pericarp and seed coat tissues maintained relatively high transcript levels encoding a variety of mitochondrial functions at 20 d after pollination. Transcripts of genes encoding chloroplast proteins were also detected, consistent with the hypothesis that photosynthetic activity in maternal tissues may supply oxygen to support metabolic demands (Rolletschek et al. 2004) (Fig. S34, Table S3).

The transcript abundance for *Translocase of the Outer Membrane* (*TOM*) *TOM40* (*HORVU4Hr1G051720*) and *TOM9* (*HORVU7Hr1G064180*), *Translocase of the Inner Membrane* (TIM) *TIM17* (*HORVU2Hr1G033040*) and *TIM50* (*HORVU3Hr1G073750*), Mitochondrial Processing Peptidase (MPP) (*HORVU1Hr1G075540*) and Intermediate Cleaving Peptidase (*ICP55*) (*HORVU6Hr1G041920*) revealed that genes encoding components for mitochondrial biogenesis are being expressed (Fig. 7, Fig. S34). Genes encoding components of the 5 multi-subunit complexes of the respiratory chain showed a more homogeneous pattern of expression between tissues and throughout development, but noting the intensity and the percentage of cells in which expression was detected did vary to some extent, even for subunits that encode proteins in the same complex. In the case of the alternative respiratory pathways in mitochondria, genes encoding components of the electron transfer flavoprotein (ETF) seemed to dominate, and also noticeably *NDB3* (*HORVU3Hr1G076920*) and *NDA1* (*HORVU3Hr1G087850*) show very specific embryo and endosperm expression at 3 and 6 d after pollination, and pistil epidermis for *NDA1*. Genes encoding components involved in glycolysis and fermentation were also highly expressed from the earliest developmental time points. For glycolysis, several genes encoding components were highly expressed at all time points, such as endolase (*HORVU5Hr1G002040*) and glyceraldehyde 3-phosphate dehydrogenase (*HORVU7Hr1G074690*), but yet another gene encoding endolase (*HORVU7Hr1G017640*) was only detected at 20 d after pollination in subaleurone. Likewise, genes encoding components involved in fermentation such as pyruvate decarboxylase (*HORVU3Hr1G018550*) display high expression at 12 and 20 d in aleurone and alcohol dehydrogenase (*ADH*) (*HORVU1Hr1G082250*) at 12 d in both endosperm clusters and at 20 d in only in endosperm3 cluster. Likewise, a distinct peak of *ADH* (alcohol dehydrogenase, *HORVU4Hr1G016810*) expression at 20 d after pollination in the scutellum and may indicate local metabolic adaptations (Fig. 7b).

During germination, greater variability in gene expression patterns for mitochondrial functions emerged. Genes encoding components involved in mitochondrial biogenesis, *TOM* and *TIM*, and mitochondrial peptidases (*MP*), peak at 3 h after imbibition in the plumule, embryo/

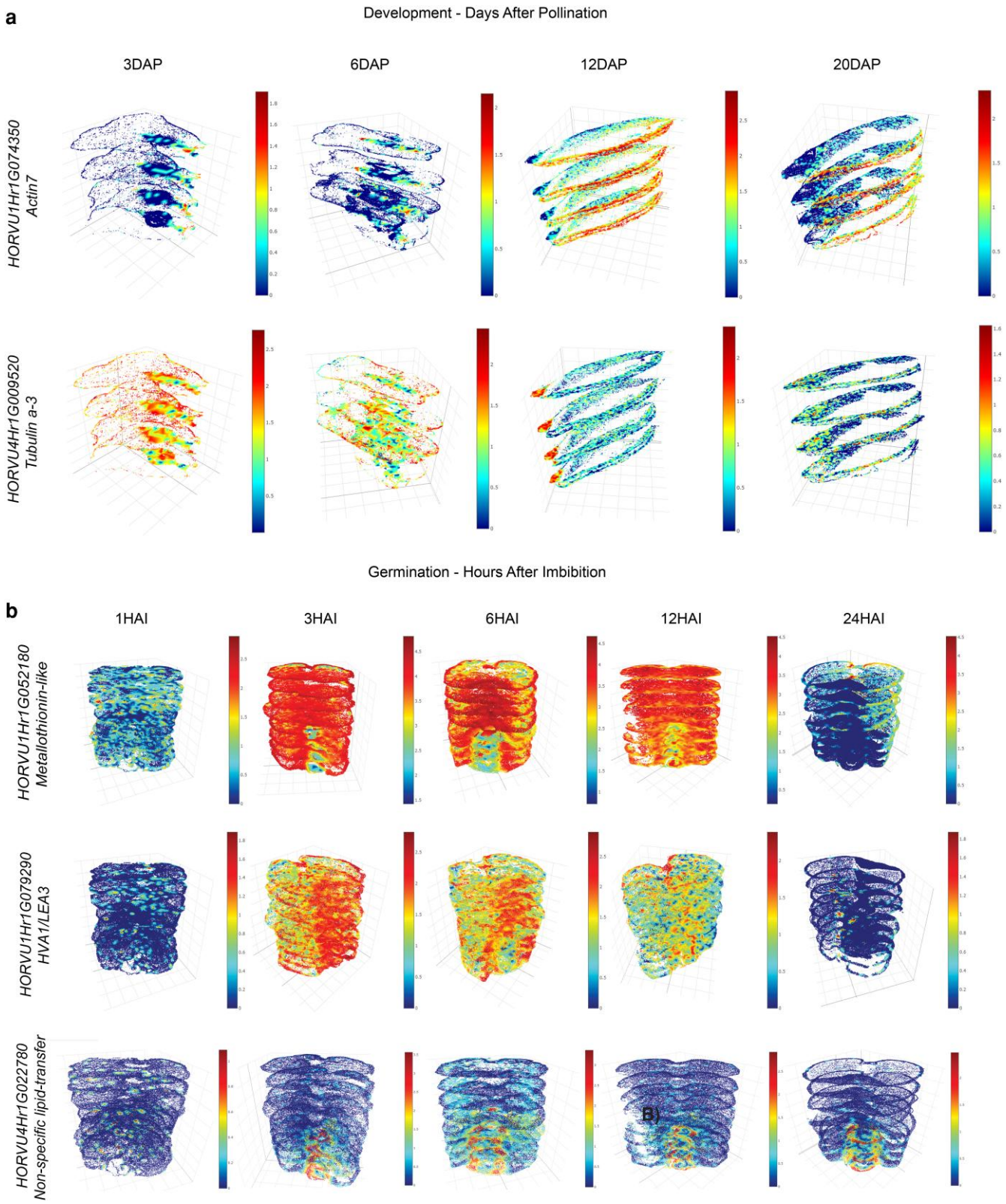

Figure 5 Three-dimensional patterns of gene expression for genes that show a homogenous pattern of expression in (a) development and (b) germination. a) The 3-D transcript abundance pattern of *Actin 7* and *Tubulin α-3* in developing barley caryopsis. b) The 3-D transcript abundance pattern of genes encoding a Metallothionin-like protein, a Late Embryogenesis protein 3 (*LEA3*) and a nonspecific lipid-transfer protein during development.

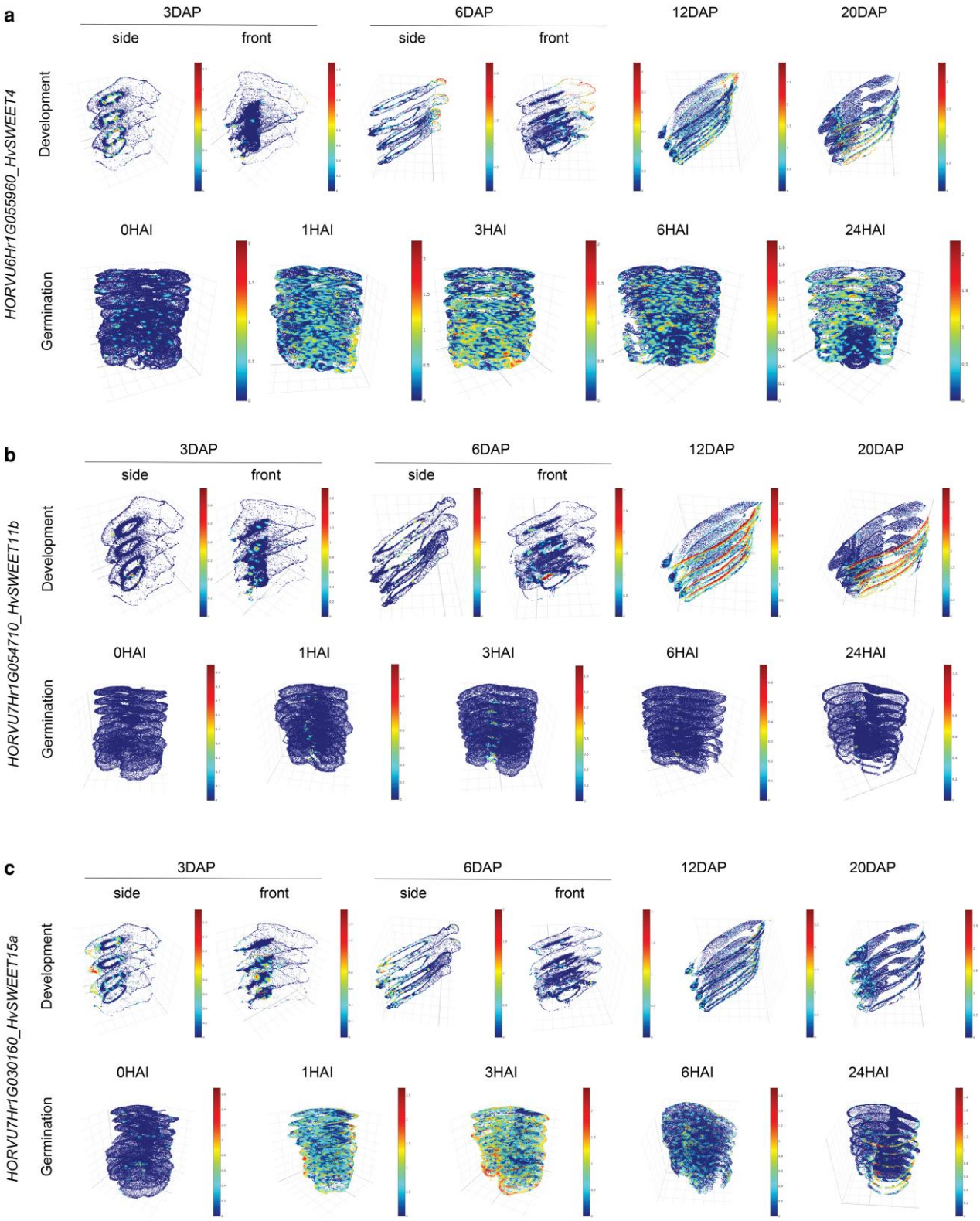

Figure 6 SWEET genes show 2- and 3-D variation during development and germination. Three-dimension reconstruction of: a) *HvSWEET4* gene during development (top), showing uniform expression at the pistil at 6 d after pollination, Chlorenchyma and ETC at 12 d after pollination and vascular bundle at 20 d after pollination and germination transverse (bottom), where the expression is mottled and scattered across the starchy endosperm and specific areas of the aleurone (black arrows). See Figures S31–S33 for 2-D spatial images. b) *HvSWEET11b* gene displayed a specific uniform pattern in nucellar projection spots at 12 and 20 d after pollination which can be only detected in remaining spots in the crease during germination. c) *HvSWEET15a* gene that showed a restricted location and mottled pattern at the bottom of the pericarp closer to the early development (3 and 6 d after pollination) and later on in embryo tissues. However, a more uniform expression pattern in the aleurone and mottled in the starchy endosperm that appeared only in the aleurone at later germination time points. Abbreviations: DAP, days after pollination; HAI, hours after imbibition.

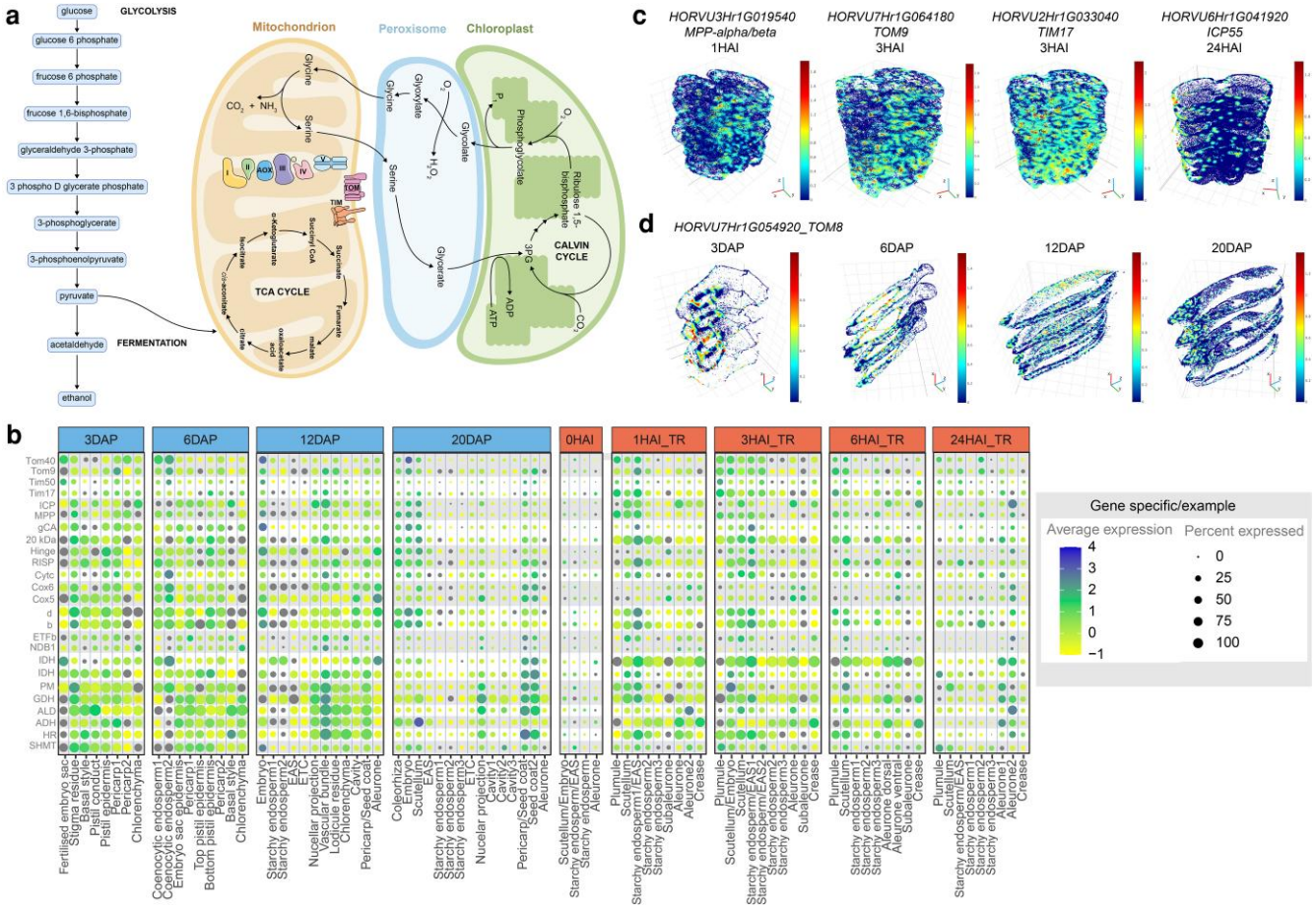

Figure 7 Transcript abundance for mitochondrial and associated functions during barley grain development and germination. a) Overview of the mitochondrial and associated functions where transcript abundance was analyzed. While glycolysis, photorespiration, and fermentation take place outside mitochondria as indicated, they were included due to direct links with mitochondrial metabolism. b) Transcript abundance for specific examples for genes encoding proteins for various activities. (see Fig. S21 function for all genes). TOM - translocase of the outer mitochondrial membrane with *Tom40* and *Tom9* representing subunit of 40 kDa and 9 kDa as examples. TIM - translocase of the inner membrane with *Tim50* and *Tim17* representing specific examples. MP - mitochondrial peptidases with *MPP* (mitochondrial processing peptidase) and *ICP*(Intermediate cleaving peptidase) representing a specific example. CI—Complex I of the mitochondrial respiratory chain with the 20 kDa subunit (*HORVU3Hr1G068360*) and γ-carbonic anhydrase (*HORVU6Hr1G044700*) as examples. CIII—Complex III of the mitochondria electron transport chain with RISP (Rieske FeS protein) (*HORVU2Hr1G071350*) and the Hinge protein (*HORVU4Hr1G020160*) as examples. Cytochrome c (*HORVU7Hr1G058850*). CV—Complex IV of the mitochondrial electron transport chain with *Cox5* (*HORVU5Hr1G023010*) and *Cox6 (HORVU2Hr1G085960)* (Cytochrome oxidase) as examples. CV—Complex V of the mitochondrial respiratory chain with the β-subunit (*HORVU1Hr1G083840*) and δ-subunit (*HORVU6Hr1G069370*) of the ATP synthase representing as example. AR—alternative electron transport pathways with *NDB1* (*alternative external NADH dehydrogenase*) (*HORVU7Hr1G101500*) and electron transfer flavoprotein (ETF) beta (*HORVU6Hr1G093180*) as examples. TCA—tricarboxylic acid cycle with 2 genes encoding *IDH (isocitrate dehydrogenase*) (*HORVU3Hr1G059060* and *HORVU2Hr1G087970*) as examples. Gly -glycolysis with *GDH (glyceraldehyde-3-phosphate dehydrogenase*) (*HORVU7Hr1G074690*) and *PM* (*phosphoglycerate mutase*) (*HORVU3Hr1G080530*) as examples. Fer—fermentation with *ADH* (*alcohol dehydrogenase*) (*HORVU4Hr1G016810*) and *ALD* (*aldehyde dehydrogenase*) (*HORVU7Hr1G042880*) as examples. PR—photorespiration with *SHMT* (*serine hydroxymethyltransferase*) (*HORVU2Hr1G110110*) and *HR* (*hydroxypyruvate reductase*) (*HORVU3Hr1G031200*) as examples. c) 3-D representation of genes expression for *MPP-alpha/beta* at 1 h after imbibition, *TOM9* at 3 h after imbibition, *TIM17* at 3 h after imbibition, and *ICP55* at 24 h after imbibition, revealing both 2-D and 3-D variation in patterns in clusters and d) *TOM8* translocator during development shows expression in the coenocytic endosperm at 3 and 6 d after pollination, embryo and starchy endosperm at 12 d after pollination and expression mainly in embryo tissues at 20 d after pollination.

scutellum, and EAS1 regions, aligning with a known burst of mitochondrial biogenesis reported in rice (Howell et al. 2006, 2007) (Fig. 7b). In contrast, starchy endosperm and aleurone tissues showed more restricted expression of biogenesis-related transcripts, though subaleurone layer at 3 and 6 h after imbibition exhibited high transcript levels in a smaller percentage of cells. Fermentation-related genes were low in endosperm clusters during germination, consistent with reduced respiratory activity. In aleurone tissues, fermentation gene expression remained relatively high, potentially reflecting the aleurone's role in secreting organic acids to maintain acidic conditions that facilitate starch hydrolysis and cell wall loosening (Ma et al. 2017) (Fig. 7b).

Photorespiration closely followed photosynthetic activity during development, peaking in tissues like the chlorenchyma, embryo sac, and early starchy endosperm at 3 and 6 d after pollination, reflecting the presence of PSI and PSII components (Fig. S35). In germination,

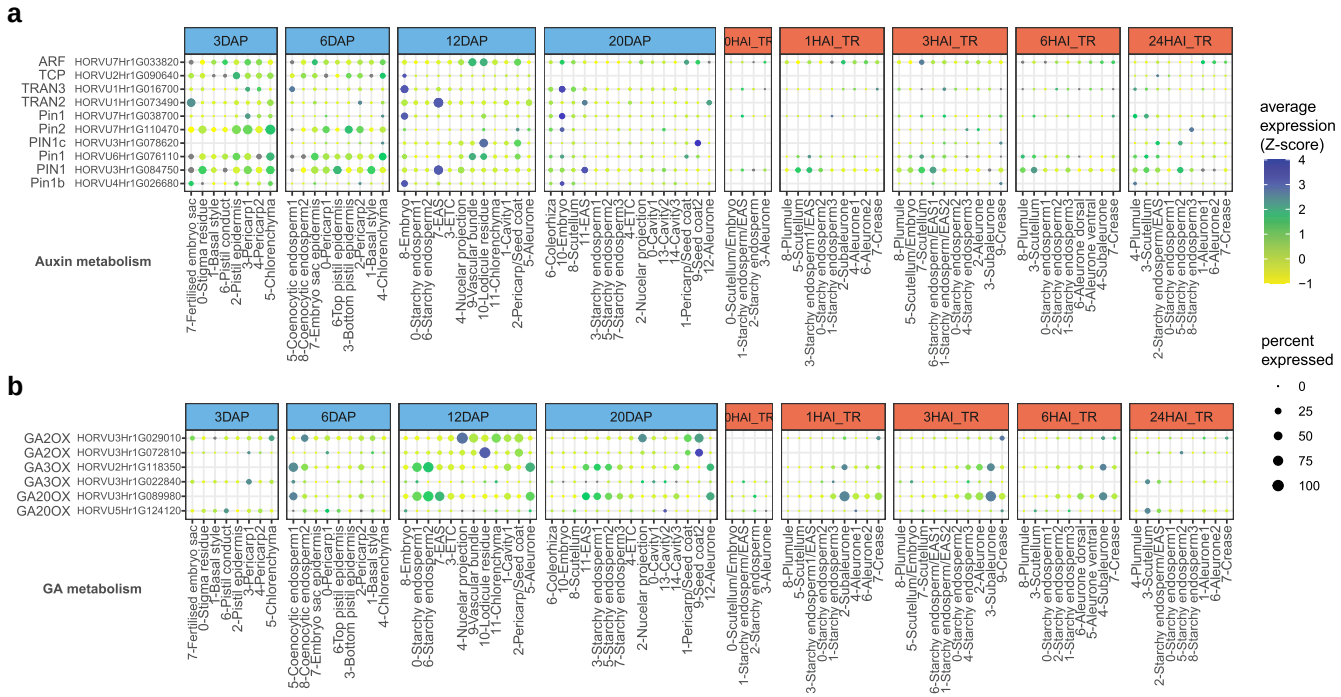

Figure 8 The pattern of expression of genes encoding proteins involved in a) Auxin metabolism and b) Gibberellic acid metabolism during development and germination. Color scale corresponds to the average gene expression across the spots per cluster and the circle size indicates the percentage of spots expressing a gene within the cluster. *ARF*, auxin response factor; *TCP*, Teosinte branched 1, Cycloidea, PCF1 (proliferating cell nuclear antigen factor 1); *Trans*, transporter-like protein; *GA2OX*, gibberellin 2-oxidase; *GA3OX*, Gibberellin 3-beta-dioxygenase, *GA20OX*, Gibberellin 20 oxidase. Annotations taken from Table S6.

photorespiratory components were evenly expressed across clusters, often peaking in aleurone or subaleurone tissues (Fig. 7b). This may indicate a role for photorespiratory enzymes (eg *GDH*, *SHMT*) in 1-carbon metabolism (Maurino and Peterhansel 2010), essential for nucleotide and hormone synthesis and other biosynthetic processes, despite the absence of detectable PSI and PSII activity (Fig. S35). For chloroplast functions, a simpler pattern emerged: photosynthetic components were primarily expressed in the chlorenchyma at 12 d after pollination (Fig. S35), with some transcription at 3 and 6 d after pollination in embryo sac and pericarp. During germination, while some plastid-associated transcripts were detected, these likely reflect enzymes involved in primary carbon metabolism rather than classical photosynthetic activity.

To visualize the 2-D and 3-D patterns in mitochondrial gene expression, we focused on 1 and 3 h after imbibition, when many components (eg *TOM*, *TIM*, *MP*, glycolysis-related genes) were expressed widely but with tissue-specific restrictions. 3-D reconstructions of mitochondrial processing peptidase (*MPP*) at 1 h after imbibition, and *TOM9*, *TIM17*, and *ICP55* at 3 h after imbibition revealed dispersed, mottled patterns of expression, often asymmetric and varying in both planar (2-D) and volumetric (3-D) dimensions (Fig. 7c; HTML Files S11–15). The asymmetric localization of *ICP55* in one side of the aleurone exemplifies this heterogeneity. Similarly, examining mitochondrial biogenesis gene *TOM8* during development showed that its expression was primarily associated with future embryo tissues, shifting spatial localization as the grain matured (Fig. 7d).

In summary, transcripts related to mitochondrial and chloroplast energy metabolism were abundant and dynamic throughout barley grain development and germination. While some genes were expressed through development and germination, others showed more restricted expression in specific clusters at restricted time points, revealing the cell/subtissue specialization of mitochondrial during seed development and germination.

Expression analysis of hormone metabolism genes reveals unprecedented spatiotemporal resolution at subtissue level

After pollination, both environmental and developmental signals mediated by hormonal signaling pathways are required for caryopsis development. All major hormones have been implicated in caryopsis development and germination (Yu et al. 2015), with auxin and GA previously shown to play central roles in pericarp growth (Pielot et al. 2015). Auxin is involved in early pericarp development, while GA functions both early and later. ABA contributes to a later role in reserve deposition and maturation (Tuan et al. 2023). Genes encoding proteins involved in ABA, GA, auxin, and brassinosteroids were expressed during development and germination and to a lesser extent for ethylene, cytokinin, salicylic acid, and jasmonate (Fig. S36).

Focusing on genes encoding auxin and GA-associated metabolism as growth drivers, we observed that auxin-related genes peaked at 3, 6, and 12 d, and were much reduced at 20 d after pollination (Fig. S36). However, the coleorhiza, embryo, and scutellum still showed noticeable expression, and a gene at locus *HORVU7Hr1G039930* encoding an oxidoreductase of unknown function remained strongly expressed in endosperm clusters (Fig. S36).

Since hormones are transported, we examined genes encoding auxin transporters. Eight genes annotated as encoding auxin transport proteins could be detected during development (Fig. 8a). While some genes displayed the expression profile at 3, 6, and 12 d after

pollination across various tissues, several showed tissue-specific expressions in embryo. These included genes encoding proteins with highest similarity to *PIN1b* at 12 and 20 d after pollination, *PIN1* in endosperm adjacent to scutellum (EAS) at 12 and 20 d after pollination, and *PIN1c* in lodicule residue and seed coat at 12 and 20 d after pollination respectively. A *Transporter like 2 protein* (*TRAN2*) was initially expressed in the fertilized embryo sac and subsequently in the EAS at 12 and 20 d after pollination (Fig. 8a). This exclusive spatiotemporal expression of these transporters provides fine resolution of how auxin promotes grain development, with these early growth stages defining grain shape and size of the grain (Pielot et al. 2015). Furthermore, the increased expression of *Dormancy marker 1/Auxin repressed protein* (DRM1/ARP, *HORVU4Hr1G011740*) at 20 d after pollination in the scutellum and aleurone, and to a lesser extent coleorhiza, reveals the fine-tuning between growth and maturation that occurs in developing grain (Fig. S36). *DRM1/ARP* has previously been characterized as barley in pre-anthesis tip degeneration of the barley inflorescence and shown to be induced by ABA (Pielot et al. 2015). While *DRM1/ARP* has been studied in bud dormancy and abiotic stress, to our knowledge its expression in seed dormancy has not been characterized (Rae et al. 2013). Its appearance at 12 d in embryo and at 20 d after pollination in coleorhiza, embryo, scutellum, EAS, and aleurone, but not in the cavity and endosperm tissues, points to tissue-specific processes occurring during grain development. During germination, while *DRM1/ARP* is expressed at 1 h after imbibition in all tissues, its plumule expression is subsequently reduced, as might be expected in a rapidly developing system.

Gibberellins (GAs) also play central roles caryopses development and germination with GA3 and GA20 oxidases essential for synthesis and GA2 oxidases involved in degradation. At 3 d, we detected both GA20 and GA3 oxidases, with *GA3ox* most strongly expressed in pericarp1 and *GA20ox* in pistil conduct cluster (Fig. 8b). Expression increased dramatically to different isoforms of both at 6 d after pollination, most noticeably in coenocytic endosperm 1 and to a lesser extent in pericarp2. Expression at 12 and 20 d was most strongly observed in endosperm clusters and aleurone. *GA2 oxidase* was also present from the earliest stages but strongest in chlorenchyma at 3 d after pollination and coenocytic endosperm 2 at 6 d. Noticeably, at 12 d after pollination, the expression patterns of synthesis vs degradation of oxidases were essentially opposite.

The *GA2* oxidases have been recently analyzed in a pan-transcriptome study of barley (Guo et al. 2025a). Expression of the gene encoding *GA2ox7* isoform was predominant in caryopsis of the variety Morex, while the gene encoding homolog *GA2ox3* displayed wider tissue and abiotic stress-induction expression. Pan-transcriptome analysis revealed variation in expression of these genes across genomes. Our analysis adds to this by showing that more than 1 gene family member is expressed in distinct tissue and subtissue patterns, which could be compared with the expression patterns of the GA synthesis gene family members, enabling targeted approaches to breed or modify expression for specific end uses.

Trajectory inference analysis reveals a comprehensive roadmap for development of aleurone tissue from early development to late germination

The aleurone layer is a specialized tissue originated from the outer layer of the endosperm playing a crucial role in the production of enzymes responsible for mobilizing starch reserves in the endosperm. We constructed a pseudotime trajectory to investigate how aleurone layer gene expression progresses in the context of development and germination, as an example of the development of tissue from early development to the completion of germination. A broad group of clusters, that encapsulated the putative aleurone lineage, was selected for the analysis (Fig. 9a and Fig. S37). The new clustering of the data by the trajectory analysis grouped the clusters at each time points together indicating the subset data retained spatiotemporal information (Fig. 9b). The early germination time points, 1, 3, and 6 h after imbibition grouped together. The reconstructed of the pseudotime trajectory was consistent with the actual experimental biological timeline (Fig. 9c).

To investigate how regulation of gene expression in the aleurone lineage changes over time, we used graph-autocorrelation for differential expression analysis, identifying genes that vary over the pseudotime trajectory. The rice *SLR1-like2* corresponds to a DELLA protein from the GRAS transcription factor that negatively regulates GA signaling pathway and *OsGAMyb-like* is a gibberellin-related MYB transcription factor in rice. Both TFs are well known for their role in response to gibberellin (GA) in cereal aleurone cells. However, their pseudotime trajectories (Fig. 9d) and spatial expression (2-D and 3-D, Fig. 9e and f) identified both GA-related TFs expressed at different points during the time course. *SLR1-like2* gene was highly expressed in the early development in the coenocytic endosperm (6 d after pollination), and aleurone expression at 12 and 20 d after pollination. Contrastingly, the barley ortholog of *OsGAMyb* was sparsely expressed during development but highly localized to the aleurone layer during germination, with spotted/mottled pattern at 24 h after imbibition (Fig. 9f). These spatial expression patterns demonstrate the timely control of GAs at the aleurone level.

We used the find_gene_modules function to define 109 distinct modules of co-expressed genes across the pseudo time trajectory of aleurone lineage (Fig. 9g and Table S4). This coexpression analysis defined 3 d after pollination modules that corresponded to the syncytial stage, 6 d after pollination modules that corresponded to the cellularization phase, 12 d after pollination modules corresponding to mid-storage, and 20 d after pollination modules corresponding to late storage. Germination was classified into early germination (1, 3, and 6 h after imbibition modules), and late germination (24 h after imbibition modules), with a group of modules shared between early and late germination (Fig. 9g). The genes are enriched in modules at 3 d after pollination (ie the pre-storage phase) corresponded to functions related to mitotic cell cycle and DNA packaging, while chloroplast-related processes were enriched at 6 d after pollination. Intermediate storage phase modules included terms related to starch metabolism and proteins targeted to endoplasmic reticulum, and late storage included a-amylase inhibitor activity, nutrient reservoir activity as well as negative regulation of proteolysis. The germination shared functions of the aleurone layer at all time points included ribosome-related and translational elongation terms, early phase of germination involved RNA modification and noncoding RNA processing and late germination involved glutathione metabolism, RNA splicing, and spliceosome complex.

Focusing on transcription factor enrichment over the aleurone development trajectory (Fig. 9h), we identified different families that were enriched at different times with known and functionally characterized factors identified along with other members of these families that have yet to have roles defined. At the pre-storage group (3 d after pollination) we found transcription gene families including *TCP*

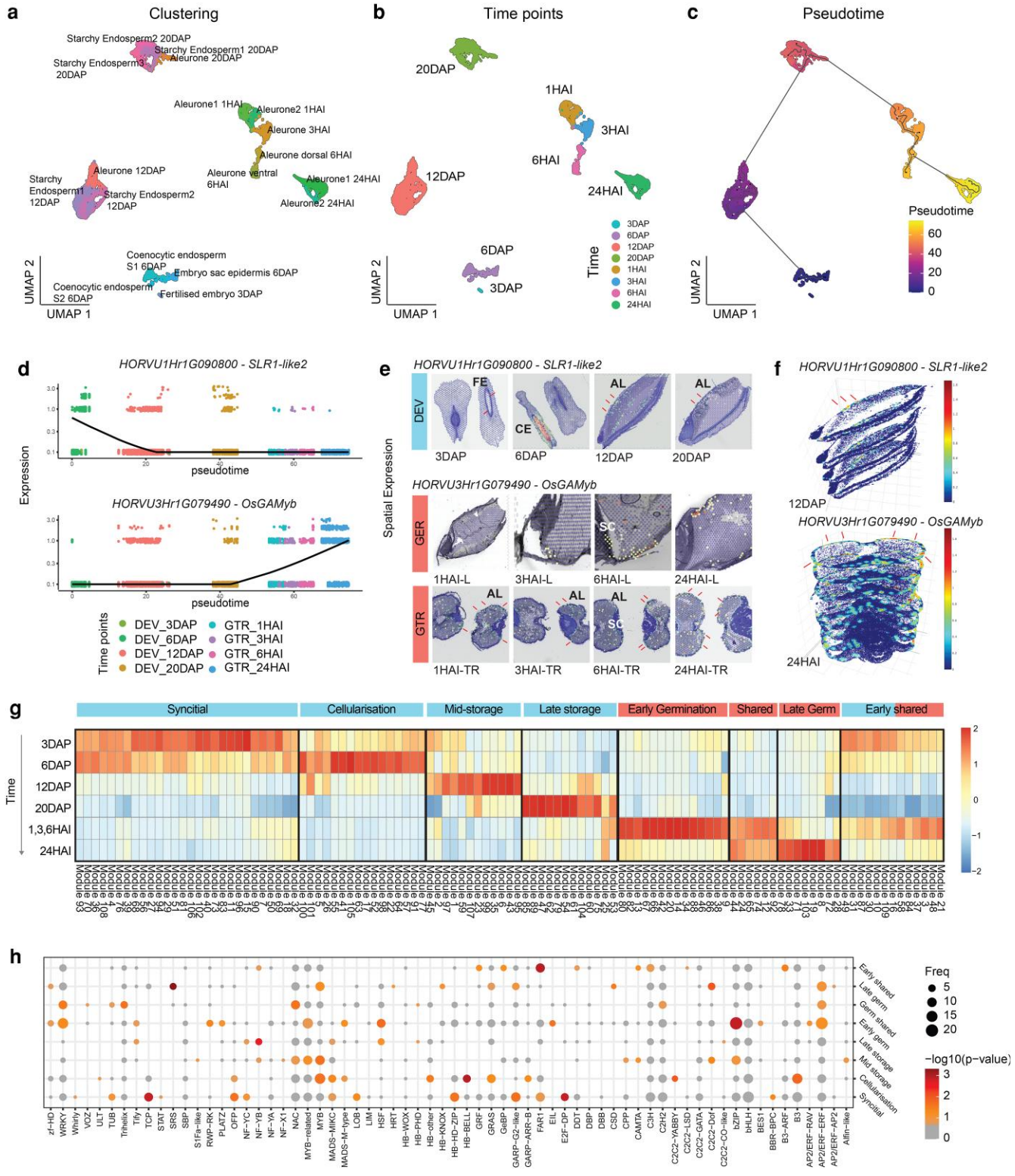

Figure 9 Trajectory analysis showed a roadmap for development of aleurone tissue from early development to late germination. a) UMAP embeddings showing the subset of clusters selected for the trajectory analysis of aleurone. b) UMAP embeddings overlaid with time points, c) UMAP embeddings showing the pseudotime trajectory of the aleurone clusters. Colour gradient indicates pseudotime. d) Expression of *SLR1-like 2* (*HORVU1Hr1G090800*) and *OsGAMyb* (*HORVU3Hr1G079490*). *OsGAMyb*, showed expression across the aleurone at all time points during germination. e) Spatial 2-D and f) 3-D transcript abundances for the transcription factors in d). Red arrows indicate the areas with observed expression. g) Heat map of the co-expression analysis for pseudotime-associated genes for aleurone lineage. Colored boxes at the top of the graph illustrate the higher order clustering that matched with the main time points in this analysis. h) Significantly enriched transcription factor (TF) families in coexpressed gene modules, grouped by developmental stage (hypergeometric test; $P < 0.05$). Circle size reflects the number of TFs per family; circle color indicates enrichment significance ($-\log_{10}$ *P*-value). Abbreviations: AL, aleurone layer; CE, coenocytic endosperm; DAP, days after pollination; FE, fertilized embryo sac; HAI, hours after imbibition; L, longitudinal, SC, scutellum; TR, transverse. Hours after imbibition-L in sagittal view; hours after imbibition-TR in cross section view.

(*Teosinte Branched 1/Cycloidea/Proliferating cell factor*), *ESF-DP* (*E2F-Dimerization Partner*), *BBR-BPC* (*Barley B-Recombinant/Basic Pentacysteine*), *TUBBY*, *NY-YC*, *LOB* (*Lateral Organ Boundaries*), and *HB-HD-ZIP* (*Homeobox-leucine zipper*) to be specifically enriched (Fig. 9h). *TCP9* reached peak expression 2 d after pollination in wheat and mutations lead to altered grain length (Zhao et al. 2018), The retinoblastoma like transcription factor (E2F-DP) specifically enriched at 3 d after pollination inhibits genes that are required for later seed maturation, thus allowing rounds of cell division in early embryo development, interacting with cyclins to control cell division, and plays an important role in monocots where endosperm development is prominent (Sabelli et al. 2013; Desvoyes and Gutierrez 2020). In Arabidopsis, this is via interaction with MADS box transcription factors that are also enriched at 3 d after pollination (Paolo et al. 2021). *LOB* transcription plays a role in early embryo development in maize (Evans 2007). *Nuclear factor Y (NF-Y)* plays essential roles in embryogenesis in Arabidopsis (Fornari et al. 2013; Mu et al. 2013) and endosperm in rice (Zhiguo et al. 2018). Many other stage specific transcription factors can also be observed such as *bZIP*, *FARL*, *WRKY*, *NACs*, etc. The ability to detect these at the earliest stages of seed development and germination, in 2-D and 3-D resolution (Fig. 9d–f), provides precise targets for investigating function, regulation and variation in genes for targeted traits, avoiding prediction approaches with bulk or even single cell/nuclei sequencing that cannot give the spatial resolution required to target specific developmental processes in a tissue and temporal manner.

Public visualization browser

As we can only select a small fraction of the data to highlight the unique insights that spatial transcriptomes can provide, we have developed the Barley 4D Gene Atlas application and hosted a public visualization browser that is running that application at the following Internet address: https://barley-4d.latrobe.edu.au/ or https://barley-4d-gene-atlas.hutton.ac.uk/. This tool allows users to explore our dataset in detail and examine their specific genes of interest, providing granular insights through various visualizations (Fig. S38). The application generates visualizations ranging from cluster analysis to 2-D and 3-D views of transcript abundance. Users can download these visualizations as PNG files, or in the case of the 3-D UMAP and 3-D transcript abundance, as HTML files. The interface includes tabs with filters to easily navigate and focus on specific datasets, timepoints, sections or genes.

Discussion

Seed development and germination represent the most intensively studied aspects of plant biology with various ‘omic’ profiling studies carried out on a variety of species (Baud et al. 2023; Liew et al. 2024; Yuan et al. 2024; Barreda et al. 2025; Zhang et al. 2025). The gene expression atlas produced in this study differs in that it is solely generated using a spatial transcriptomic approach. This provides quantitative transcript abundance of over 20,000 genes in a 3-D spatial context over caryopsis development and germination. A variety of transcript abundance patterns were observed, from homogeneity in the 2-D and 3-D axes to variation across both planes. Variation was observed as expected between and within clusters, as has been observed in a variety of other studies using sc/sn/sp RNA-seq. In the limited spatial studies published in plants, heterogeneity in gene expression has been observed across different technologies. For example, a spatial study of plant immunity revealed that immune-active zones were not uniformly distributed and showed dynamic patterns over time (Hu et al. 2025). These zones responded to the proximity of virulent bacteria, indicating that gene expression at the cellular level is highly responsive to local stimuli (Nobori et al. 2025). Similarly, spatial transcriptomics of the developing maize ear uncovered cell subtypes consisting of only a few layers (Wang et al. 2024). Overall, both abiotic and biotic responses in plants are heterogeneous at the cellular level (Tenorio Berrío and Dubois 2024). Likewise at a transcriptional level, heterogeneity has been observed using *in vivo* real-time visualization of transcription (Alamos et al. 2021; Hani et al. 2021). It was observed that the response to heat stress or Pi limitation displayed remarkable heterogeneity between adjacent cells, and that essentially a limited number of cells are responsible for the increases that are observed when such stimuli are applied. That is essentially what we have observed here in terms of transcript abundance for some but notably not all genes.

An emerging concept in plant biology studies is the recognition that tissues may be in a hypoxic state in ambient aerobic conditions due to limited diffusion and consumption of oxygen. It has been shown that young leaves in Arabidopsis undergo cyclic hypoxia due to high rates of oxygen consumption (Triozzi et al. 2024). In particular in developing and germinating seeds, high respiratory demand has led to the conclusion that “oxygen deficiency is the normal condition in developing seeds” (Rolletschek et al. 2024), with hypoxic signaling evident and signature gene expression in both seed development and germination. Thus, the heterogeneity of gene expression observed in this study for genes associated with starch metabolism and mitochondrial function, that are both highly energy demanding processes, may be a result of the micro-environmental conditions caused by high oxygen demand and limited diffusion.

Variation in gene expression at a cellular level has been shown to be important for development in both animal and plant systems (Maranas and Nemhauser 2025). Transcriptional “noise” as it has been termed, has been observed in mammalian blastocyst and Drosophila development and sepal development in plants. Stochastic expression of the transcription factor SPEECHLESS guides epidermal cells to a stomatal cell lineage. Noisy gene expressions may be under dynamic gene body regulation. Stochastic processes that may be maintained or amplified dynamically by environmental or micro-environmental conditions (Cortijo and Locke 2020). Starch breakdown requires the secretion of amylases from the scutellum and aleurone, which means it cannot instantly be homogenous over the whole endosperm. However, as starch metabolism requires O_2 due to the high energy demand, this will become limiting, due to the high rate of consumption and reduced diffusion in relatively dense plant tissues (Holdsworth et al. 2024). Thus, developmental processes combined with micro-environment conditions may maintain and amplify the heterogeneous genes expression patterns for some genes.

While spatial transcriptome approaches have the promise to provide cell-based spatial resolution of gene expression, there are limitations in this study. We and others have shown the veracity of this technology previously (Peirats-Llobet et al. 2023), and this is further supported by examples that, for specific genes, the expression pattern we observed here closely matched those reported in earlier studies in barley using gene-specific traditional approaches (such as GUS staining and *in situ* hybridization) (Radchuk et al. 2023; Yue et al. 2023). However, a key limitation is that only a small portion of the grain could be sampled in development and germination, due to the

extremely high costs of the technology. It is worth noting that this study includes several replicates, which remains uncommon in spatial studies to date due to the same cost limitations. Future advances in technology will enable 3-D cellular resolution across entire tissues and organs, as has been demonstrated in low-throughput (Nobori 2025). Furthermore, the current resolution of 55 μm clearly is larger than a single cell. Even so, the emerging picture highlights specific candidate genes in both time and space, offering valuable targets for functional genomics and also prompts further investigations using diverse spatial technologies to visualize 3-D transcript profiles of genes during development.

A further limitation of this study was that it focused only on protein coding transcripts. Other RNA molecules, such as microRNA which can be mobile and provide communication between cells, tissues and organs (Gao et al. 2025), as well as cell specific *cis* motifs that drive gene expression, were not profiled (Marand et al. 2025; Zhang et al. 2025). Studies combining single cell transcriptomics and accessible chromatin regions across species provide a roadmap for applying or translating the ability to obtain cell specific spatiotemporal expression of desired genes (Mendieta et al. 2024). Finally, but not least, single cell approaches are now being applied to proteins and metabolites (Montes et al. 2024; Ntelkis et al. 2025). While a recent study showed that DNA codon frequencies and transcript abundance were the main predictors of protein abundance (Zhong et al. 2025), a combination of multiple single cell 'omic' profiles, from epigenome, proteome, to metabolite profiling would greatly enhance the understanding of how cell types contribute to whole plant growth and development.

Materials and methods

Spatial transcriptomics tissue preparation

Plant growth and tissue processing

For the development dataset, barley grains (cv La Trobe) were grown on standard potting mix in the glasshouse with 22 °C/18 h light during the day and 16 °C/6 h during the night conditions. Grains (3 to 4), at the indicated time points, were collected from the middle of the tillers and immediately froze in liquid nitrogen until blocks were generated. For the germination dataset, grains were surface sterilized using chlorine-gas method in a fume hood, germinated on 2 of 2 layers of sterilized paper filter with 12 mL of sterile water added and wrapped in foil at 23 °C. Grains were harvested at the indicated time points. Tissue sections for both datasets were prepared as previously described in Peirats-Llobet et al. 2023 with minor modifications. Briefly, the cryoblocks were cut to a thickness of 8 μm and the sections were placed onto the Visium slides. The Visium gene expression slides were incubated in the thermocycler at 37 °C for 1 min, fixed with chilled methanol at −20 °C for 30 min, stained with 0.05% Toluidine Blue in water with 2 U/μl RNase inhibitor at room temperature (RT) before imaged with the Axioscan 7 slide scanner (Zeiss).

Library construction and sequencing

Libraries from the different capture areas on the Visium Gene Expression slide were synthesized as described in 10× user guide (PN-1000190, CG000239_VisiumSpatialGeneExpression_UserGuide_RevD). Visium libraries were sequenced on an Illumina NextSeq 550 platform according to the 10× Genomics Visium manufacturer's instructions (NextSeq 500/550 High Output kit v2.5 (150 cycles) 20024907, CG000239_VisiumSpatialGeneExpression_UserGuide_RevD), targeting 100 million reads using dual indexing kit TT set A (PN-1000215, 10× Genomics).

Spatial gene expression analysis

Data processing

High resolution brightfield images were loaded into Loupe browser software (v 7.1 10× Genomics), fiducial frames were manually adjusted, and the area covered by tissue was selected using the lasso tool. The resulting Loupe files were used to generate alignment files for each section. Barley genome (International Barley Sequencing Consortium v2.51) served as a reference genome for aligning the sequencing reads. The alignment files, sequencing data, and bright field images were subsequently utilized as input for Space Ranger (v2.1.1 10× Genomics) to generate gene-spot matrices. The quality control of the data was performed in a way that filtered out spots with fewer than 200 UMI counts or fewer than 150 genes for the developmental dataset and with fewer than 30 UMI counts or fewer than 10 genes for the germination transverse dataset. For each time point, the data from 4 sections were consolidated with the "merge" function from the Seurat package (v4.4.0). Also, the read count normalization and clustering were done with the same Seurat package. Subsequently, SCTransform from the Seurat package was employed to normalize the data for the developmental dataset with the following parameters: assay = "Spatial", variable.features.n = NULL, return.only.var.genes = FALSE. For the generation transverse dataset, the additional parameter vars.to.regress = c('section') for SCTransform is used.

Clustering and cell type annotation

The optimal number of principal components (PCs) was determined to be 75 for the developmental dataset and 103 for the germination transverse dataset by plotting the deviations of the principal components using runPCA and ElbowPlot functions and calculating the percent of variation associated with each PC. UMAP dimensionality reduction was performed with the RunUMAP function using the parameters reduction = "pca" and dims = 1:75 for the developmental and dims = 1:103 for the germination transverse dataset. To identify the clusters, FindNeighbours and FindClusters functions were utilized with the parameter's dims = 75 for developmental and dims = 103 for germination transverse, resolution = 0.4/0.3/0.3/0.5 for individually analyzed developmental dataset, and resolution = 0.9/0.4/0.5/0.5/0.3 for germination transverse individual datasets, while keeping other parameters at their defaults. Marker genes for each of the clusters were identified using the function FindAllMarkers (settings: min.pct = 0.05, logfc.threshold = 0.25, only.pos = TRUE, test.use = "wilcox"). To annotate the identified clusters, the top 10 genes in each cluster were identified, followed by a Gene Ontology analysis (http://bioinformatics.sdstate.edu/go77/), and inspection their spatial locations using the SpatialFeaturePlot function.

3-D reconstruction

The STUtility (version 1.1.1) R package was used to perform 3-D reconstruction of spatial transcriptomics data with integrated gene expression. The 3-D reconstruction consisted of 2 steps: preparing data and creating a 3-D stack. Data preparation combined the filtered feature matrix (spatial gene expression), brightfield images of the tissue, tissue coordinates and tissue positions using the InputFromTable function. Custom masks of the brightfield images were generated for each time point. Manual selection of spots covered by tissues was

performed for each of the time points. In the case of 3 and 6 d after pollination, the capture areas contained 2 sections corresponding to 2 different grains and the spots were processed separately and generated individual.rds files for each segment. For germination transverse data, the capture areas contained 2 sections but, in this case, they were serial sections from the same grain and were processed as individual segments, however combined in the final.rds file. The segmented.rds files were merged for the respective timepoints and generated 6 .rds files for development and 5 .rds files for germination transverse datasets. Creation of the 3-D stack involved alignment (order, angle and position of the sections respect to axis x and y) of the brightfield images in the.rds files per timepoint, using the function ManualAlignImages. Create3DStack function was run (with parameters limit = 1, maxnum = 20e3, and nx = 500). FeaturePlot3D function (mode = "cloud") was used to display the spatial gene expression pattern for the genes of interest.

Mitochondrial and chloroplast gene expression profiles

The Mapman annotations for barley were used to extract the gene information for mitochondrial and plastid proteins (chloroplast) (Sreenivasulu et al. 2008; Tables S2 and S6). For mitochondria this encompasses genes encoding respiratory chain subunits (complex I to V), cytochrome c biogenesis, components involved in alternative respiration and the TCA cycle. For chloroplasts this encompassed genes encoding proteins of the Calvin cycle, chloroplastic glycolysis, PSI, PSII, cytochrome b_6f and chloroplast, ATP synthase and NADH dehydrogenases. The translocases and peptidases responsible for protein import, processing and assembly were annotated directly by blasting the verified Arabidopsis genomic sequences against the barley genome. Blast results with an e score $<2e^{-5}$ were selected and annotated identifying 13 genes encoding Translocase of the Outer Mitochondrial membrane (*TOM*), 28 genes encoded Translocase of the Inner Mitochondrial Membrane (*TIM*), and 16 genes encoding mitochondrial peptidases (*MP*). For Chloroplasts, 21 genes encoding Translocases of outer envelope membrane of chloroplasts (*TOC*), 19 genes encoding Translocases of inner envelope membrane of chloroplasts (*TIC*) and 11 genes encoding chloroplasts import components (CIC) were identified. Additionally, the proteins associated with fermentation and photorespiration were included. Overall, 300 genes that encoded mitochondrial components were detected in 1 or more of the 130 clusters that are generated with low resolution clustering of the datasets. Likewise, for plastids/chloroplasts, this resulted in more than 150 genes encoding components of the light and dark reaction of photosynthesis (Figs. S34 and S35).

For each multi-subunit protein complex or pathway associated with mitochondria the expression level of 2 genes from that complex is shown (Fig. 7), with the full quantitative visualization for all genes shown in Figures S34 and S35.

Trajectory inference analysis

The Monocle3 (version 1.3.1) R package was used to perform the trajectory analysis. First, the clusters corresponding to annotated aleurone tissues from all the timepoints were extracted and reprocessed. Briefly, the data (gene expression, genes and spots metadata) was used to construct a monocle object which was reprocessed using the custom parameters (preprocess_cds (num_dim = 60), align_cds (alignment_k = 25), reduce_dimension (umap.n_neighbors = 50) and cluster_cells) were executed. The analysis clustered the aleurone tissues in 6 partitions that corresponded well with the time points. The next step was to call the functions learn_graph(), using use_partition = FALSE to and order_cells, which allowed manual choosing of root nodes (since our data has a temporal component, 3 d after pollination clusters were used as starting node). Graph-autocorrelation analysis was then carried out to find genes that vary as a function of pseudotime using the graph_test() function, followed by find_gene_modules(-neighbor_graph="principal_graph") to identify modules of co-regulated genes across the groups. Gene Ontology analysis was performed using ShinyGO 0.77 (http://bioinformatics.sdstate.edu/go77/).

Public visualization application

The application for the Barley 4D Gene Atlas was built with Shiny, a web framework based on Python and available for R (https://shiny.posit.co/py/docs/comp-r-shiny.html). The Barley 4D Gene Atlas application enables the user to view 3 datasets: Development, Germination Longitudinal, and Germination Transverse. It features plots for UMAP, Clustering, and Transcript Abundance. The user can use filters in the application to select which dataset, timepoint, section, and gene they would like to see plots for. They are also able to download the plots generated by the application. By default, it shows the data of the study, but a user can also use the application with their own data. The code required to run the application on a local computer is available in this public GitHub repository: https://github.com/4D-Barley-Spatial-Transcriptomics/Barley-4D-Gene-Atlas-Public. To run it locally, the user must first download the code from the link. In the directory named "User Guide", the user can find the PDF detailing the steps to be able to run the app. They must first take the *.h5 file and filtered_feature_bc_matrix/features.tsv from SpaceRanger and run it through the pipeline detailed in the user guide. This pipeline will create input files for the application. Note that a computer with at least 64 GB of RAM is required to run the application.

Accession numbers

All accession numbers are shown on Figures S13 to S36 and Tables S2, S3 and S6.

Acknowledgments

We would like to thank Dr Lim Chee Liew and Lucas Auroux for their suggestions and reading the manuscript. This study was supported by the La Trobe University Genomics Platform. The author(s) responsible for distribution of materials integral to the findings presented in this article in accordance with the policy described in the Instructions for Authors (https://academic.oup.com/plcell/pages/General-Instructions) are James Whelan (jimwhelan@zju.edu.cn) and Marta Peirats-Llobet (M.Peirats-Llobet@latrobe.edu.au).

Author contributions

MP-L, MGL, and JW conceived and designed the study. MP-L carried out experimental procedures, and MP-L, ZS, and JW carried out the primary analysis, with MP-L, MGL, XY, MRT, HS, and JW defining and annotating clusters. MP-L, CH, YZ, MWM, VM, and GAK interrogated and interpreted the data for energy biology metabolism. MP-L, BH, GAK, MGL, and JW carried out the trajectory analysis. FA, MSLY, MP-L, ZS, HS, RZ, IM, and JW designed and implemented the visualizations of 2-D and 3-D gene expression patterns and database. MP-L and

JW drafted the first version of the manuscript, that was edited by all authors.

Supplementary material

Supplementary material is available at *The Plant Cell* online.

Funding

Funding provided by Bioplatforms Australia Limited under the project "Cutting edge Mass Spectrometry and expertise at the La Trobe University Institute for Sustainable Agriculture and Food (LISAF)", La Trobe University and DVCRIE.

Conflicts of interest

None declared.

Data availability

The spRNA-seq data are available in GEO accession GSE294392. To review GEO accession GSE294392: Go to https://www.ncbi.nlm.nih.gov/geo/query/acc.cgi?acc=GSE294392. Enter token ozqfmwwgbvevbab into the box. The public visualization browser is available at the following Internet address: https://barley-4d.latrobe.edu.au/or https://barley-4d-gene-atlas.hutton.ac.uk/. The code required to run the visualization application on a local computer is available in this public GitHub repository: https://github.com/4D-Barley-Spatial-Transcriptomics/Barley-4D-Gene-Atlas-Public.

References

Alamos S, Reimer A, Niyogi KK, Garcia HG. 2021. Quantitative imaging of RNA polymerase II activity in plants reveals the single-cell basis of tissue-wide transcriptional dynamics. Nat Plants. 7:1037–1049. https://doi.org/10.1038/s41477-021-00976-0.

An YQ, Lin L. 2011. Transcriptional regulatory programs underlying barley germination and regulatory functions of gibberellin and abscisic acid. BMC Plant Biol. 11:105. https://doi.org/10.1186/1471-2229-11-105.

Armenta-Medina A et al. 2021. Developmental and genomic architecture of plant embryogenesis: from model plant to crops. Plant Commun. 2:100136. https://doi.org/10.1016/j.xplc.2020.100136.

Auroux L, Liew LC, Whelan J, Lewsey MG. 2025. Advances in seed 'omics. J Exp Bot. 77:2045–2058. https://doi.org/10.1093/jxb/eraf294.

Barreda L et al. 2025. Specialized metabolome and transcriptome atlas of developing *Arabidopsis thaliana* seed under warm temperatures. Sci Data. 12:306. https://doi.org/10.1038/s41597-025-04563-2.

Basto S et al. 2015. Long-term nitrogen deposition depletes grassland seed banks. Nat Commun. 6:6185. https://doi.org/10.1038/ncomms7185.

Baud S et al. 2023. Recent progress in molecular genetics and omics-driven research in seed biology. C R Biol. 345:61–110. https://doi.org/10.5802/crbiol.104.

Bellamy AS et al. 2024. United Kingdom Food security report 2024. UK Government.

Betts NS et al. 2020. Transcriptional and biochemical analyses of gibberellin expression and content in germinated barley grain. J Exp Bot. 71:1870–1884. https://doi.org/10.1093/jxb/erz546.

Bewley JD, Bradford KJ, Hilhorst HW, Nonogaki H et al. 2013. Dormancy and the control of germination. In: Seeds: Physiology of Development, Germination and Dormancy. 3rd edn. Springer New York. p. 247–297. https://doi.org/10.1007/978-1-4614-4693-4.

Collins HM et al. 2021. Genes that mediate starch metabolism in developing and germinated barley grain. Front Plant Sci. 12:641325. https://doi.org/10.3389/fpls.2021.641325.

Cortijo S, Locke JCW. 2020. Does gene expression noise play a functional role in plants? Trends Plant Sci. 25:1041–1051. https://doi.org/10.1016/j.tplants.2020.04.017.

Cuesta-Seijo JA et al. 2017. Functional and structural characterization of plastidic starch phosphorylase during barley endosperm development. PLoS One. 12:e0175488. https://doi.org/10.1371/journal.pone.0175488.

Desvoyes B, Gutierrez C. 2020. Roles of plant retinoblastoma protein: cell cycle and beyond. EMBO J. 39:e105802. https://doi.org/10.15252/embj.2020105802.

Eskelinen A, Elwood E, Harrison S, Beyen E, Gremer JR. 2021. Vulnerability of grassland seed banks to resource-enhancing global changes. Ecology. 102:e03512. https://doi.org/10.1002/ecy.3512.

Evans MM. 2007. The indeterminate gametophyte1 gene of maize encodes a LOB domain protein required for embryo sac and leaf development. Plant Cell. 19:46–62. https://doi.org/10.1105/tpc.106.047506.

Fornari M, Calvenzani V, Masiero S, Tonelli C, Petroni K. 2013. The Arabidopsis NF-YA3 and NF-YA8 genes are functionally redundant and are required in early embryogenesis. PLoS One. 8:e82043. https://doi.org/10.1371/journal.pone.0082043.

Fu Y et al. 2023. Spatial transcriptomics uncover sucrose post-phloem transport during maize kernel development. Nat Commun. 14:7191. https://doi.org/10.1038/s41467-023-43006-7.

Gao Z et al. 2025. Cell-type specific miRNA regulatory network responses to ABA stress revealed by time series transcriptional atlases in Arabidopsis. Adv Sci (Weinh). 12:e2415083. https://doi.org/10.1002/advs.202415083

Giacomello S et al. 2017. Spatially resolved transcriptome profiling in model plant species. Nat Plants. 3:17061. https://doi.org/10.1038/nplants.2017.61.

Guo W et al. 2025a. A barley pan-transcriptome reveals layers of genotype-dependent transcriptional complexity. Nat Genet. 57:441–450. https://doi.org/10.1038/s41588-024-02069-y.

Guo X et al. 2025b. An Arabidopsis single-nucleus atlas decodes leaf senescence and nutrient allocation. Cell. 188:2856–2871.e16. https://doi.org/10.1016/j.cell.2025.03.024.

Hani S et al. 2021. Live single-cell transcriptional dynamics via RNA labelling during the phosphate response in plants. Nat Plants. 7:1050–1064. https://doi.org/10.1038/s41477-021-00981-3.

Holdsworth MJ et al. 2024. Geography, altitude, agriculture, and hypoxia. Plant Physiol. 197:kiae535. https://doi.org/10.1093/plphys/kiae535.

Howell KA et al. 2007. Oxygen initiation of respiration and mitochondrial biogenesis in rice. J Biol Chem. 282:15619–15631. https://doi.org/10.1074/jbc.M609866200.

Howell KA, Millar AH, Whelan J. 2006. Ordered assembly of mitochondria during rice germination begins with pro-mitochondrial structures rich in components of the protein import apparatus. Plant Mol Biol. 60:201–223. https://doi.org/10.1007/s11103-005-3688-7.

Hu Y et al. 2025. Spatial and single-cell transcriptomics capture two distinct cell states in plant immunity. Front Plant Sci. 16:1637176. https://doi.org/10.3389/fpls.2025.1637176

Huang L, Tan H, Zhang C, Li Q, Liu Q. 2021. Starch biosynthesis in cereal endosperms: an updated review over the last decade. Plant Commun. 2:100237. https://doi.org/10.1016/j.xplc.2021.100237.

Kong D et al. 2022. Combined RNA-Seq and phenotype analysis reveals a potential molecular mechanism of the difference in grain size of naked barley from the Qinghai-Tibetan plateau. Front Plant Sci. 13:822607. https://doi.org/10.3389/fpls.2022.822607.

Kovacik M et al. 2024. The transcriptome landscape of developing barley seeds. Plant Cell. 36:2512–2530. https://doi.org/10.1093/plcell/koae095.
Law SR et al. 2012. Nucleotide and RNA metabolism prime translational initiation in the earliest events of mitochondrial biogenesis during Arabidopsis germination. Plant Physiol. 158:1610–1627. https://doi.org/10.1104/pp.111.192351.
Lee TA et al. 2025. A single-cell, spatial transcriptomic atlas of the Arabidopsis life cycle. Nat Plants. 11:1960–1975. https://doi.org/10.1038/s41477-025-02072-z.
Li X, Schmitz RJ. 2025. Cis-regulatory dynamics in plant domestication. Trends Genet. 41:984–994. https://doi.org/10.1016/j.tig.2025.02.005.
Liew LC et al. 2024. Establishment of single-cell transcriptional states during seed germination. Nat Plants. 10:1418–1434. https://doi.org/10.1038/s41477-024-01771-3.
Liu C et al. 2022a. A spatiotemporal atlas of organogenesis in the development of orchid flowers. Nucleic Acids Res. 50:9724–9737. https://doi.org/10.1093/nar/gkac773.
Liu J, Wu MW, Liu CM. 2022b. Cereal endosperms: development and storage product accumulation. Annu Rev Plant Biol. 73:255–291. https://doi.org/10.1146/annurev-arplant-070221-024405.
Logan DC, Millar AH, Sweetlove LJ, Hill SA, Leaver CJ. 2001. Mitochondrial biogenesis during germination in maize embryos. Plant Physiol. 125:662–672. https://doi.org/10.1104/pp.125.2.662.
Ma Z, Bykova NV, Igamberdiev AU. 2017. Cell signaling mechanisms and metabolic regulation of germination and dormancy in barley seeds. Crop J. 5:459–477. https://doi.org/10.1016/j.cj.2017.08.007.
Maranas C, Nemhauser JL. 2025. Building resilience by cultivating difference: a role for noise in development. Curr Opin Plant Biol. 88:102809. https://doi.org/10.1016/j.pbi.2025.102809.
Marand AP et al. 2025. The genetic architecture of cell type-specific cis regulation in maize. Science. 388:eads6601. https://doi.org/10.1126/science.ads6601.
Maurino VG, Peterhansel C. 2010. Photorespiration: current status and approaches for metabolic engineering. Curr Opin Plant Biol. 13:248–255. https://doi.org/10.1016/j.pbi.2010.01.006.
Mendieta JP et al. 2024. Investigating the cis-regulatory basis of C(3) and C(4) photosynthesis in grasses at single-cell resolution. Proc Natl Acad Sci. 2024;121:e2402781121. https://doi.org/10.1073/pnas.2402781121
Minow MAA, Marand AP, Schmitz RJ. 2023. Leveraging single-cell populations to uncover the genetic basis of Complex traits. Annu Rev Genet. 57:297–319. https://doi.org/10.1146/annurev-genet-022123-110824.
Montes C, Zhang J, Nolan TM, Walley JW. 2024. Single-cell proteomics differentiates Arabidopsis root cell types. New Phytol. 244:1750–1759. https://doi.org/10.1111/nph.19923.
Moreno-Villena JJ et al. 2022. Spatial resolution of an integrated C(4)+CAM photosynthetic metabolism. Sci Adv. 8:eabn2349. https://doi.org/10.1126/sciadv.abn2349.
Mu J, Tan H, Hong S, Liang Y, Zuo J. 2013. Arabidopsis transcription factor genes NF-YA1, 5, 6, and 9 play redundant roles in male gametogenesis, embryogenesis, and seed development. Mol Plant. 6:188–201. https://doi.org/10.1093/mp/sss061.
Narsai R et al. 2017. Extensive transcriptomic and epigenomic remodelling occurs during *Arabidopsis thaliana* germination. Genome Biol. 18:172. https://doi.org/10.1186/s13059-017-1302-3.
Nobori T. 2025. Exploring the untapped potential of single-cell and spatial omics in plant biology. New Phytol. 247:1098–1116. https://doi.org/10.1111/nph.70220.
Nobori T et al. 2025. A rare PRIMER cell state in plant immunity. Nature. 638:197–205. https://doi.org/10.1038/s41586-024-08383-z.
Ntelkis N, Buell CR, Goossens A. 2025. Plant metabolism: zoom into the single-cell level. Plant Physiol. 199:kiaf375. https://doi.org/10.1093/plphys/kiaf375.
Oliva M, Lister R. 2023. Exploring the identity of individual plant cells in space and time. New Phytol. 240:61–67. https://doi.org/10.1111/nph.19153.
Olsen OA. 2001. ENDOSPERM DEVELOPMENT: cellularization and cell fate specification. Annu Rev Plant Physiol Plant Mol Biol. 52:233–267. https://doi.org/10.1146/annurev.arplant.52.1.233.
Paolo D et al. 2021. The Arabidopsis MADS-domain transcription factor SEEDSTICK controls seed size via direct activation of E2Fa. Plants. 10:192. https://doi.org/10.3390/plants10020192.
Paszkiewicz G, Gualberto JM, Benamar A, Macherel D, Logan DC. 2017. Arabidopsis seed mitochondria are bioenergetically active immediately upon imbibition and specialize via biogenesis in preparation for autotrophic growth. Plant Cell. 29:109–128. https://doi.org/10.1105/tpc.16.00700.
Peirats-Llobet M et al. 2023. Spatially resolved transcriptomic analysis of the germinating barley grain. Nucleic Acids Res. 51:7798–7819. https://doi.org/10.1093/nar/gkad521.
Pielot R et al. 2015. Hormone-mediated growth dynamics of the barley pericarp as revealed by magnetic resonance imaging and transcript profiling. J Exp Bot. 66:6927–6943. https://doi.org/10.1093/jxb/erv397.
Poutanen KS et al. 2022. Grains - a major source of sustainable protein for health. Nutr Rev. 80:1648–1663. https://doi.org/10.1093/nutrit/nuab084.
Radchuk VV et al. 2009. Spatiotemporal profiling of starch biosynthesis and degradation in the developing barley grain. Plant Physiol. 150:190–204. https://doi.org/10.1104/pp.108.133520.
Radchuk VV et al. 2023. SWEET11b transports both sugar and cytokinin in developing barley grains. Plant Cell. 35:2186–2207. https://doi.org/10.1093/plcell/koad055.
Rae G, David K, Wood M. 2013. The dormancy marker DRM1/ARP associated with dormancy but a broader role in planta. Developmental Biology Journal. 2013:1–12. https://doi.org/10.1155/2013/632524.
Rani H, Bhardwaj RD. 2021. Quality attributes for barley malt: "the backbone of beer". J Food Sci. 86:3322–3340. https://doi.org/10.1111/1750-3841.15858.
Rolletschek H, Borisjuk L, Gómez-Álvarez EM, Pucciariello C. 2024. Advances in seed hypoxia research. Plant Physiol. 197:kiae556. https://doi.org/10.1093/plphys/kiae556.
Rolletschek H, Weschke W, Weber H, Wobus U, Borisjuk L. 2004. Energy state and its control on seed development: starch accumulation is associated with high ATP and steep oxygen gradients within barley grains. J Exp Bot. 55:1351–1359. https://doi.org/10.1093/jxb/erh130.
Sabelli PA et al. 2013. Control of cell proliferation, endoreduplication, cell size, and cell death by the retinoblastoma-related pathway in maize endosperm. Proc Natl Acad Sci U S A. 110:E1827–E1836. https://doi.org/10.1073/pnas.1304903110.
Sreenivasulu N et al. 2008. Barley grain maturation and germination: metabolic pathway and regulatory network commonalities and differences highlighted by new MapMan/PageMan profiling tools. Plant Physiol. 146:1738–1758. https://doi.org/10.1104/pp.107.111781.
Tenorio Berrío R, Dubois M. 2024. Single-cell transcriptomics reveals heterogeneity in plant responses to the environment: a focus on biotic and abiotic interactions. J Exp Bot. 75:5188–5203. https://doi.org/10.1093/jxb/erae107.
Tremblay BJM et al. 2024. Interplay between coding and non-coding regulation drives the Arabidopsis seed-to-seedling transition. Nat Commun. 15:1724. https://doi.org/10.1038/s41467-024-46082-5.

Triozzi PM et al. 2024. Spatiotemporal oxygen dynamics in young leaves reveal cyclic hypoxia in plants. Mol Plant. 17:377–394. https://doi.org/10.1016/j.molp.2024.01.006.

Tuan PA, Nguyen TN, Toora PK, Ayele BT. 2023. Temporal and spatial transcriptional regulation of phytohormone metabolism during seed development in barley (*Hordeum vulgare* L.). Front Plant Sci. 14:1242913. https://doi.org/10.3389/fpls.2023.1242913.

Wang W et al. 2025. Single-cell and spatial transcriptomics reveals a stereoscopic response of rice leaf cells to *Magnaporthe oryzae* infection. Adv Sci (Weinh). 12:e2416846. https://doi.org/10.1002/advs.202416846.

Wang Y et al. 2024. A spatial transcriptome map of the developing maize ear. Nat Plants. 10:815–827. https://doi.org/10.1038/s41477-024-01683-2.

Xia K et al. 2022. The single-cell stereo-seq reveals region-specific cell subtypes and transcriptome profiling in Arabidopsis leaves. Dev Cell. 57:1299–1310.e4. https://doi.org/10.1016/j.devcel.2022.04.011.

Yan H et al. 2025. A single-cell rice atlas integrates multi-species data to reveal cis-regulatory evolution. Nat Plants. 11:2050–2071. https://doi.org/10.1038/s41477-025-02106-6.

Yao J et al. 2024. Spatiotemporal transcriptomic landscape of rice embryonic cells during seed germination. Dev Cell. 59:2320–2332.e5. https://doi.org/10.1016/j.devcel.2024.05.016.

Yu SM, Lo SF, Ho TD. 2015. Source-sink communication: regulated by hormone, nutrient, and stress cross-signaling. Trends Plant Sci. 20:844–857. https://doi.org/10.1016/j.tplants.2015.10.009.

Yuan X et al. 2024. Integrative omics analysis elucidates the genetic basis underlying seed weight and oil content in soybean. Plant Cell. 36:2160–2175. https://doi.org/10.1093/plcell/koae062.

Yue W, Cai K, Xia X, Liu L, Wang J. 2023. Genome-wide identification, expression pattern and genetic variation analysis of SWEET gene family in barley reveal the artificial selection of HvSWEET1a during domestication and improvement. Front Plant Sci. 14:1137434. https://doi.org/10.3389/fpls.2023.1137434.

Zhang X et al. 2025. A spatially resolved multi-omic single-cell atlas of soybean development. Cell. 188:550–567.e19. https://doi.org/10.1016/j.cell.2024.10.050.

Zhao J et al. 2018. Genome-wide identification and expression profiling of the TCP family genes in spike and grain development of wheat (*Triticum aestivum* L.). Front Plant Sci. 9:1282. https://doi.org/10.3389/fpls.2018.01282.

Zhiguo E et al. 2018. A group of nuclear factor Y transcription factors are sub-functionalized during endosperm development in monocots. J Exp Bot. 69:2495–2510. https://doi.org/10.1093/jxb/ery087.

Zhong Z et al. 2025. The distinct roles of genome, methylation, transcription, and translation on protein expression in *Arabidopsis thaliana* resolve the Central Dogma's information flow. Genome Biol. 26:319. https://doi.org/10.1186/s13059-025-03741-0.

Zhu Y et al. 2020. Conserved and opposite transcriptome patterns during germination in Hordeum vulgare and *Arabidopsis thaliana*. Int J Mol Sci. 21:7404. https://doi.org/10.3390/ijms21197404.